THE UNIVERSITY OF CALGARY

AN RF FEEDBACK AMPLIFIER FOR LOW INTERMODULATION DISTORTION PERFORMANCE

BY

JOHN GODFREY McRORY

A THESIS SUBMITTED TO THE FACULTY OF GRADUATE STUDIES IN PARTIAL FULFILLMENT OF THE REQUIREMENTS FOR THE DEGREE OF MASTER OF ENGINEERING

DEPARTMENT OF ELECTRICAL AND COMPUTER ENGINEERING

CALGARY, ALBERTA

APRIL, 1993

The University of Calgary

Faculty of Graduate Studies

The undersigned certify that they have read, and recommend to the Faculty of Graduate Studies for acceptance, a dissertation entitled, "*An RF Feedback Amplifier for Low Intermodulation Distortion Performance*" submitted by John Godfrey McRory in partial fulfillment of the requirements for the degree of Master of Engineering.

Ronald H. Johnston

Supervisor, Dr. R. H. Johnston
Department of Electrical and Computer Engineering

Michel Fattouche

Dr. M. Fattouche
Department of Electrical and Computer Engineering

Dr. A. B. Sesay
Department of Electrical and Computer Engineering

W. Svrcek

Dr. W.Y. Svrcek
Department of Chemical and Petroleum Engineering

Date: April 22, 1993

Abstract

This thesis deals with the linearization of nonlinear amplifiers through the application of negative feedback. Conventional feedback reduces the level of the harmonic and intermodulation products by a factor equal to the loop gain, and it also causes a decrease in the overall circuit gain with a subsequent loss of output power. A modified negative feedback circuit is proposed which provides the same level of linearization as the negative feedback circuit without reducing the output power level.

The transfer function of the nonlinear amplifier is represented through a Volterra series. Analysis of the negative feedback circuit and the modified circuit are carried out using both the Volterra series and linear system analysis, and performance predictions are made. An experimental circuit is designed and tested in order to confirm the analysis. Limitations on the circuit's usable bandwidth, stability, and loop gain are derived.

Acknowledgement

I would like to acknowledge my supervisor Dr. Ron Johnston for his guidance during the course of this work. I would also like to acknowledge Dr. Paul Camwell, who's encouragement and support set me on the path.

This thesis is dedicated to my wife Kim, and to Katie and Meg. Thanks for your understanding and support for all the times I couldn't be there.

Table of Contents

List of Tables

List of Figures

List of Symbols and Abbreviations

Chapter 1

dc	direct current
DSP	Digital Signal Processing
LAN	Local Area Network
QAM	Quadrature Amplitude Modulation
QPSK	Quadrature Phase Shift Keying
RF	Radio Frequency

Chapter 2

A	feedback amplifier gain
α	envelope feedback input coupling factor
a_1	envelope feedback modulator gain
a_2	envelope feedback amplifier gain
AM	Amplitude Modulation
B	feedback loop transfer function
β	envelope feedback output coupling factor
C	feedback amplifier tuned cavity transfer function
CPL	Cubic Predistortion Linearizer
dB	logarithmic ratio of powers, ie. 10 log (power1/power2)
dBc	logarithmic ratio with respect to carrier power
E(t)	general modulation signal
e_{im}	feedback amplifier intermodulation products
e_{in}	feedback amplifier input voltage
E_m	maximum value of the general modulation signal
e_o	feedback amplifier output voltage

G	envelope feedback circuit gain
G	LINC amplifier gain
γ	envelope feedback modulator sensitivity = da_1/dV_c
η	envelope feedback rectification efficiency of detectors
I	signal component in phase
IF	intermediate frequency
LINC	Linear Amplification with Nonlinear Components
LO	Local Oscillator
MByte	megabyte of random access memory
PA	Power Amplifier
PM	Phase Modulation
Q	signal component in quadrature
RAM	Random Access Memory
$S_{1a}(t)$	+'ve phase modulated general bandpass signal
$S_{2a}(t)$	-'ve phase modulated general bandpass signal
$S_a(t)$	general bandpass signal
UHF	Ultra High Frequency
V_c	envelope feedback modulator control voltage
V_i	envelope feedback input signal level
V_{in}	RF cuber input signal
V_o	envelope feedback output signal level from amplifier
V_o	RF cuber output signal
$V_o(t)$	LINC amplifier output signal

Chapter 3

$2f_1 - 2f_2$	second order intermodulation product

$2f_1 - f_2$	third order intermodulation product
$2f_2 + f_1$	third order intermodulation product
$2\omega_1 - 2\omega_2$	second order intermodulation product
$2\omega_1 - \omega_2$	third order intermodulation product
$2\omega_2 + \omega_1$	third order intermodulation product
$3\omega_1$	third harmonic of the first two tone test fundamental
$3\omega_2$	third harmonic of the second two tone test fundamental
A	power series input voltage amplitude
dBm	dB with respect to 1 mWatt
$f_1 + f_3$	second order intermodulation product
f_1	first fundamental input tone for a two tone test
f_2	second fundamental input tone for a two tone test
G	amplifier gain
G_{1dB}	amplifier 1 dB compression point gain
G_o	amplifier linear gain
IM_3	third order intermodulation product
k_n	power series nth order coefficient
$P(2\omega_1-\omega_2)$	nonlinear amplifier third order intermodulation product output power
$P(\omega_1)$	nonlinear amplifier first fundamental output power
$P_{intercept}$	nonlinear amplifier third order intercept point
P_{linear}	linear amplifier output power
θ	phase angle
R	amplifier input impedance
t_d	group delay
$v_i(t)$	power series input voltage

$v_0(t)$	power series output voltage
ω	angular frequency
$\omega_1 + \omega_3$	second order intermodulation product
ω_1	first fundamental input tone for a two tone test
ω_2	second fundamental input tone for a two tone test

Chapter 4

(a,b)	system memory
A	scalar constant
$A(\varepsilon)$	nonlinear amplifier characteristic
A_k	amplitude of kth input exponential
b	feedback signal
$\beta(f)$	feedback loop response
B_1	third order nonlinear transfer function at ω_1
B_2	third order nonlinear transfer function at $2\omega_1-\omega_2$
ε	feedback error signal
F	any given functional
G	feedback amplifier total response
$G_1(f)$	feedback amplifier's first order Volterra kernel
$G_2(f_1,f_2)$	feedback amplifier's second order Volterra kernel
$G_3(f_1,f_2,f_3)$	feedback amplifier's third order Volterra kernel
G_n	feedback amplifier nth order Volterra kernel
H	Volterra series
h'_n	symmetrized nth order Volterra kernel
$H'_n(\omega_1, \omega_2,..., \omega_n)$	symmetrized nth order nonlinear transfer function
$H_3(-j\omega_1, j\omega_1, j\omega_1)$	third order Volterra kernel at ω_1

$H_3(-j\omega_2, j\omega_2, j\omega_1)$	third order Volterra kernel at ω_1
h_n	nonlinear amplifier's nth order Volterra kernel
h_n	nth order Volterra kernel
$H_n(\omega_1, \omega_2,..., \omega_n)$	nth order frequency domain Volterra kernel
K	number of input exponentials
m	integer index of the frequency mix for the nth order transfer function
n	order of the Volterra series kernel
S	any deterministic system
t	time
u	time delay
ωo	output frequency from nonlinear transfer function
x(t)	system input signal
$X(\omega)$	Fourier transform of x(t)
x_k	system inputs
$y_{(2\omega_1-\omega_2)}(t)$	total response at $2\omega_1-\omega_2$
y(t)	system output signal
$Y(\omega)$	nonlinear transfer function
$y_{(\omega_1)}(t)$	total response at ω_1
$y_3(\omega_1)$	third order nonlinear transfer function for ω_1
y_k	system outputs
y_n	nth order impulse response
$Y_n(\omega)$	nth order nonlinear transfer function
$y_{\omega_o}(t)$	nth order impulse response for frequency $\omega_o(t)$

Chapter 5

$\Sigma1$	input combiner
$\Sigma2$	input splitter
$\Sigma3$	cancellation combiner
$\Sigma4$	amplifier combiner
$H(f)$	feedback loop characteristic
τ_1	first delay
τ_2	second delay
τ_δ	relative delay, $\tau_2 - \tau_1$
n	number of the cancellation null
f_o	normalized center frequency
BW	circuit 3 dB bandwidth
f_{upper}	upper 3 dB frequency
f_{lower}	lower 3 dB frequency
a	splitter/combiner loss,
H	Amplifier gain and delay characteristic, $H=he^{-j\omega\tau_h}$,
c	directional coupler attenuation,
d	lower path delay, $e^{-j\omega\tau_d}$,
f	variable attenuation,
B	loop amplifier and loop filter characteristic, $B(f)e^{-j\omega\tau_b}$,
η	intermodulation products.
V_{in}	amplifier input voltage
V_{out}	amplifier output voltage
p	lowpass frequency variable
s	frequency domain variable
Q	circuit Q, defined as 1/BW

$\beta(s)$	bandpass filter with delay and gain response
FR4	fiberglass circuit board
f_c	bandpass filter center frequency
C_o	dielectric resonator equivalent parallel capacitance
L_o	dielectric resonator equivalent parallel inductance
R	dielectric resonator equivalent parallel resistance
C_p	bandpass filter parallel coupling capacitor
C_s	bandpass filter series coupling capacitor
λ	wavelength
S_{11}	S parameter input return loss
S_{21}	S parameter transfer function
MHz	Megahertz
$H_3(f_1,f_1,-f_1)$	third order Volterra kernel for f_1
$H_3(f_2,f_1,-f_2)$	third order Volterra kernel for f_1
$H_1(f_1)$	first order Volterra kernel for f_1

Chapter 6

$\Delta(f_1)$	reduction in fundamental with the application of feedback
$\Delta(2f_1\text{-}f_2)$	reduction in third order intermodulation product with the application of feedback
B_1	loop equation for f_1
B_3	loop equation for $2f_1 - f_2$

Chapter One

Introduction

The unprecedented growth in demand for wireless services that has developed over the last decade has created an urgent need for a more efficient use of the available RF spectrum. Services such as cellular radio, cordless telephones, or wireless LANs are continuously called upon to pass more information through their respective channels without exceeding their bandwidth allotment. In response to these pressures, the wireless industry has begun to focus on linear digital modulation schemes such as QAM or QPSK which are highly bandwidth efficient, but which also place more stringent requirements on the system hardware.

One of the key hardware circuits in the transmission of digital signals is the output power amplifier. The market demand for small, battery powered digital wireless terminals places conflicting linearity and efficiency demands upon this particular component. An amplifier's efficiency is a measure of the circuit's ability to convert dc power to RF power, which in the case of the battery powered terminal translates directly into battery life. However, in order to achieve an efficient operating condition the amplifier must be operated in its nonlinear region, which causes unacceptable levels of distortion in the linear digital modulation schemes.

In response to these incompatible requirements, a great deal of research has focused on the linearization of mildly nonlinear amplifiers. The techniques that have been developed allow the amplifier to operate in a more efficient nonlinear region by reducing the level of intermodulation distortion. Although both analog and digital techniques have been proposed, digital schemes such as Cartesian Feedback or Adaptive Pre-distortion offer a superior level of performance, but at the cost of substantially increased system complexity. The digital linearization schemes work at baseband, and require a significant amount of additional hardware, including down conversion in the feedback loop, demodulation of the output signal, and a significant level of DSP in order to perform the linearization.

In an effort to reduce the complexity of the linearization, an investigation of analog linearization techniques was undertaken and a new circuit proposed, developed and tested. The goals for the circuit were that it must be simple to implement, it should operate at RF frequencies in order to eliminate the requirements for additional down conversion and baseband processing, and that it should offer a significant level of improvement in circuit performance.

Analog linearization can be achieved through the use of either negative feedback or feedforward techniques. Although the feedforward technique has shown good success in broadband linearization, it requires the use of two high power amplifiers as well as the combining of two high power signals at the circuit output. Alternatively, negative feedback offers a reduction of the distortion products equal to the circuit's loop gain, but also causes a reduction of the overall circuit gain thus resulting in a lower achievable output power for a given level of distortion. In an attempt to develop a circuit that avoides these two problems, a modified feedback circuit is developed that uses the feedforward cancellation technique in a negative feedback configuration. This circuit has been demonstrated to offer a linearization equal to that of the negative feedback amplifier, but does not suffer from the subsequent gain reduction.

This thesis deals with the design, analysis and testing of the modified negative feedback circuit. Chapter 2 offers a summary of the linearization techniques available to date with brief descriptions of their operating principles, and introduces the modified feedback circuit. Chapter 3 details the distortion mechanisms present in amplifiers and the figures of merit used to characterize them. Chapter 4 introduces the power series and the Volterra series representation of nonlinear amplifiers, and then covers the Volterra series analysis of the negative feedback amplifier. Chapter 5 contains the design and linear system analysis of the experimental circuit, while Chapter 6 contains the results and measurements of the experiments carried out to confirm the analysis. Chapter 7 summarizes the experimental results and conclusions, and closes with suggestions for future work.

Chapter Two

Linearization Techniques for Nonlinear Amplifiers

The steadily increasing traffic load on the present cellular telephone networks has created a need for more efficient use of the available spectrum. Multi-level digital modulation schemes such as 64 or 256 QAM offer improved spectral efficiency, but cannot be utilized partially due to the effects of distortion introduced by the nonlinear power amplifiers used in the radios.

Traditionally power amplifiers have been optimized for efficiency, operating in the saturation region of the amplifier performance curves. This results in a highly nonlinear amplifier operation which generates several types of distortion in the output signal. These distortions include AM to AM conversion, AM to PM conversion, as well as harmonics and orthogonal intermodulation products caused by both the AM to AM and AM to PM conversions. Further variations in performance can be caused if the amplifier is operated in the mobile environment, with severe temperature variations, and changes in the electrical length of the amplifier due to the change in frequency during hand-offs.

Several methods have been proposed to linearize microwave and RF amplifiers, using either feedback control or intermodulation cancellation techniques. The focus of this section of the thesis is the review of the four methods that have been developed to deal with nonlinear amplifier operation, and to introduce the proposed modified feedback amplifier.

2.1) Feed-Forward

The feed-forward system was first developed in the late 1920's by

Harold S. Black. The system requires complex circuitry, and as such has been primarily limited to larger systems which can afford the extra complexity.

A functional diagram of the feedforward circuit is shown in Figure 2.1 [1]. Its operating principle is the reduction of the amplifier's distortion through the cancellation of the unwanted signal harmonics at the output of the circuit. An error signal is developed by comparing a delayed version of the input signal with an attenuated version of the nonlinear amplifier's output signal. The error signal is then amplified by the auxiliary amplifier and added to the main amplifier output in such a fashion that the unwanted intermodulation products are canceled, and only the amplified original signal remains.

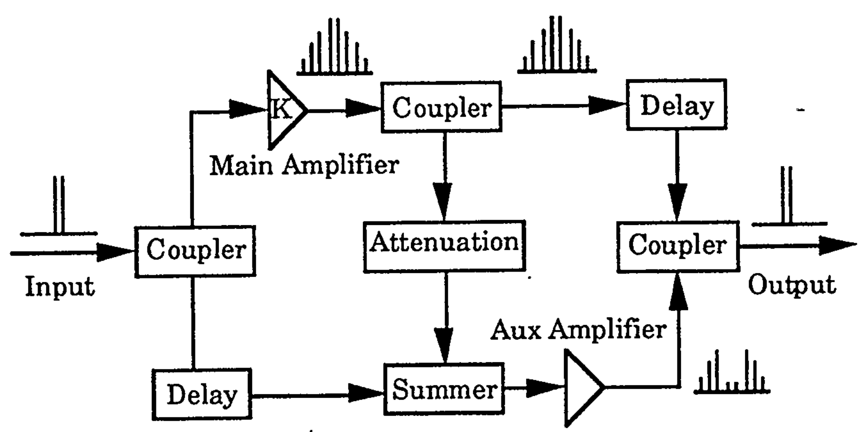

Figure 2.1 Feedforward Linearization Circuit

As shown in Figure 2.1, two input test tones are fed by the input coupler to the nonlinear main amplifier and the first time delay. The delay device compensates for the group delay inherent in the main amplifier, second coupler, and attenuator, as well as adjusting the phase of the input signal such that cancellation of the test tones occurs at the summer. The output of the nonlinear amplifier, containing the amplified input tones as well as odd order intermodulation products and AM to PM intermodulation products, is sampled and fed to the summer where it is added to the delayed input signal. The level and phase of the two signals are adjusted such that the input tones cancel, resulting in an error signal which contains primarily the unwanted intermodulation components. The error signal is then scaled and recombined with a delayed version of the main amplifier output at the output coupler. The error signal scaling and the main amplifier signal delay are optimized so that when the signals are combined the intermodulation products are canceled and the output spectrum is thus an amplified replica of the input spectrum.

The disadvantages of the Feed-Forward network are: the circuit is an open loop system, and so cannot be easily compensated for drift and temperature variations; the maximum null of the intermodulation distortion occurs at a single frequency, and is not a measure of the systems overall capability; and the circuit complexity. Further disadvantages are that the auxiliary amplifier must have approximately the same output power capacity as the main amplifier, and that the output combiner must linearly combine the two high power output signals without adding any additional distortion products.

The advantages of the feed-forward network are that the open-loop architecture is unconditionally stable, and that large reductions in distortion can be achieved, with reported results as high as 25 dB for the third order intermodulation products in a class A amplifier [2], and a 15 dB improvement for a class C amplifier [3].

2.2) Linear Amplification with Nonlinear Components (LINC)

LINC, or linear amplification with nonlinear components, is a recent extension of the outphasing technique developed by Chireix in the 1930's which was used to improve the linearity and efficiency of AM broadcast transmitters [4]. The technique allows the use of highly nonlinear components in the amplifier stages, such as class C, D, or E, and then cancels the distortion products at the circuit output through signal phasing. Raab [4] has shown that the resulting efficiency is approximately equal to that of the class of amplifier used. Like the feedforward technique, LINC does not use a feedback from the output of the power amplifier to perform the linearization, resulting in an unconditionally stable system.

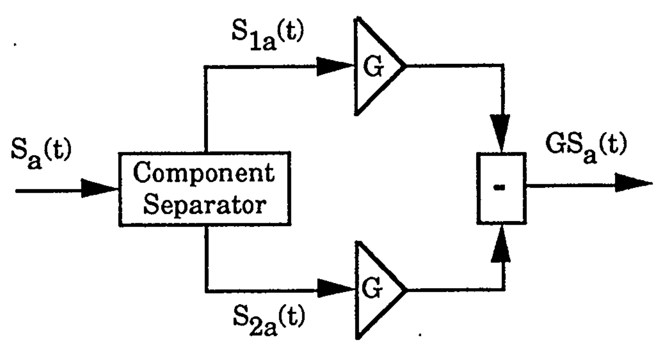

Figure 2.2 LINC Amplifier

The block diagram is shown in Figure 2.2. The principle of operation is that the bandpass input signal $S_a(t)$, which may have both amplitude and phase variations, is split into two constant envelope phase modulated signals, either by analog techniques [5] or by DSP [6]. The two constant envelope signals are then fed to a pair of identical nonlinear RF amplifiers and the amplifier outputs combined. The constant envelope signals derived from the modulation signal $S_a(t)$ are generated such that when the signals are combined at the output, the distortion products cancel and the desired signals reinforce.

If a general bandpass input signal is used such as

$$S_a(t) = E(t)\cos(\omega t + \theta(t)) \tag{2.1}$$

Cox's analysis [5] defines E(t) as

$$E(t) = E_m \sin[\phi(t)] \tag{2.2}$$

The component separator generates two sinusoidal signals with phase modulations of $+\phi(t)$ and $-\phi(t)$, such that

$$\begin{aligned} S_{1a}(t) &= \frac{E_m}{2}\sin(\omega t + \theta(t) + \phi(t)) \\ S_{2a}(t) &= \frac{E_m}{2}\sin(\omega t + \theta(t) - \phi(t)) \end{aligned} \tag{2.3}$$

The two signals are then amplified and passed through the combiner which takes the difference between the two signals, yielding

$$\begin{aligned} V_o(t) &= GS_{1a}(t) - GS_{2a}(t) \\ &= G\frac{E_m}{2}\{\sin[\omega t + \theta(t) + \phi(t)] - \sin[\omega t + \theta(t) - \phi(t)]\} \\ &= GE_m\{\cos[\omega t + \theta(t)]\sin[\phi(t)]\} \\ &= GS_a(t) \end{aligned} \tag{2.4}$$

which is simply an amplified version of the input signal, while canceling the distortion products at the summing junction.

The difficulties in this approach are the generation of the required phase modulated signals $S_{1a}(t)$ and $S_{2a}(t)$, the design of two identical amplifier chains, and the design of a method which will combine the two high power output signals from the amplifiers without introducing further nonlinear distortion products.

2.3) Feedback Linearization

Amplifier linearization using feedback can be carried out at either RF frequencies or at baseband, and can be either analog or a combination of analog and DSP techniques. All these techniques share common characteristics in the use of the feedback loop with its inherent delays, which can give stability problems and can limit the effective bandwidth of the amplifier.

2.3.1) RF Negative Feedback

Negative feedback is a well known technique for reducing distortion in linear amplifiers, but its use at UHF or microwave frequencies requires very careful treatment of the loop delay and loop bandwidth.

A typical circuit configuration is shown in Figure 2.3 [1]. Since the feedback loop can contain several cycles of delay from the input to the output, a single tuned, band limiting filter is included in the loop. The filter characteristic, feedback loss, and amplifier gain must be chosen such that the loop gain is less than one for all frequencies that could lead to an unstable operating condition.

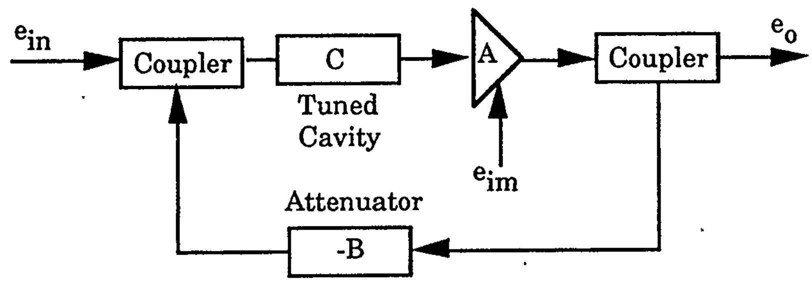

Figure 2.3 Microwave Feedback Amplifier

The analysis of the circuit in Figure 2.3 can be simplified if it is assumed that the amplifier is linear and that the distortion products are simply added to the amplifier output, and also that the second order interactions are small enough to be neglected. These assumptions allow the use of linear system theory for the analysis of the circuit. Consider the response of the circuit blocks, where A, B, and C are the transfer functions of the amplifier, feedback path including the input and output couplers, and the filter respectively. The closed loop gain for the input signal, e_{in}, can be written as

$$e_o = \frac{AC}{1+ABC} e_{in} + \frac{1}{1+ABC} e_{im} \tag{2.5}$$

Thus the intermodulation products are reduced by 1/(1 + ABC) and the overall amplifier gain is reduced by C/(1 + ABC). It can be seen that the reduction of the intermodulation products is numerically equal to the loop gain.

The factor (1 + ABC) is determined by the trade offs that must be made between the loop gain, phase margin, and the operating bandwidth, resulting in a narrow system bandwidth. A further disadvantage is the reduction of the amplifier gain resulting in additional gain being required in the output amplifier.

2.3.2) Active Feedback Linearization

The active feedback linearizer was presented in 1988 by Ballesteros, Perez, and Perez [7]. An improvement of the passive RF negative feedback, this linearizer extends the dynamic range of the feedback amplifier by adaptively adjusting the loop gain to compensate for the main amplifier's signal compression.

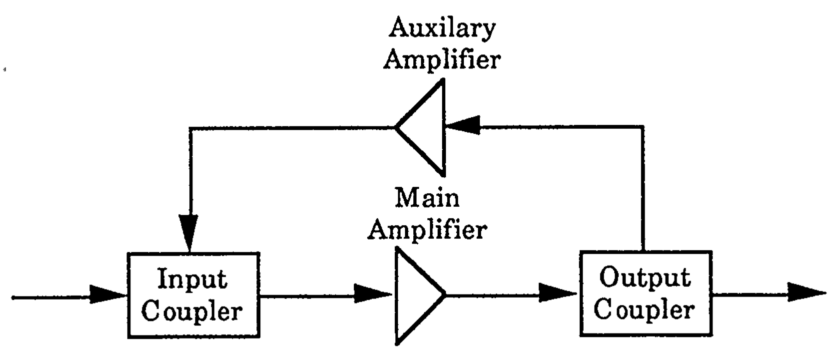

Figure 2.4 Active Feedback Linearized Amplifier

A qualitative understanding of the linearizer operation can be obtained by considering the instantaneous transfer characteristics of the main and auxiliary amplifiers. As the input signal increases in power, the main amplifier enters compression, which reduces the loop gain for the circuit. The loop gain is also affected through the coupling ratios of the input and output couplers, which scales the feedback signal such that the compression degree of the auxiliary amplifier compensates for the main amplifier's signal compression. In other words, as the auxiliary amplifier is forced into compression, the feedback loop gain is reduced which increases the overall circuit gain. The increase in the overall circuit gain compensates for the reduced output power of the main amplifier which increases the circuit's linear dynamic range. Ballesteros et al [7] report a 3.2 dB improvement in output power for a fixed level of distortion for a 1 GHz amplifier. They also report that the structure is sensitive to temperature variations since the change in the gain of the active devices impairs the performance of the circuit.

2.3.3) Envelope Feedback

Another application of feedback for amplifier linearization is envelope feedback. In this case, as shown in Figure 2.5 [8], the basis of the technique is to compare the envelope of the input signal with the envelope of the distorted output signal, and to control the instantaneous gain of the amplifier such that the differences between the envelopes are minimized.

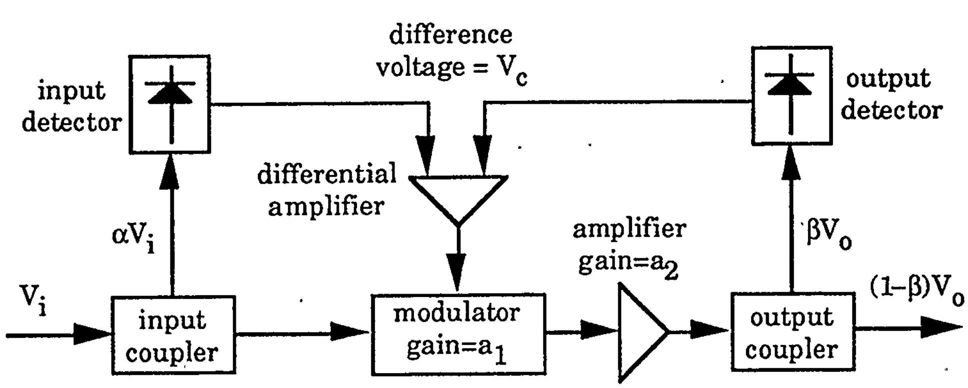

Figure 2.5 Envelope Feedback Linearizer

Figure 2.5 shows the block diagram of the circuit. If the variables are defined as:

a_1 = gain of modulator,

a_2 = gain of amplifier,

γ = modulator sensitivity = da_1/dV_c,

V_c = modulator control voltage,

V_i = input signal level,

V_o = output signal level from amplifier,

α = input coupling factor,

β = output coupling factor,

η = rectification efficiency of detectors,

then Arthanayake and Wood [8] have shown that the circuit gain with envelope feedback can be written as

$$G = \frac{(1-\beta)a_2(a_1+\alpha\eta\gamma V_i)}{(1+a_2\beta\eta\gamma V_i)} \tag{2.6}$$

If the limit of this expression is found as γ goes to infinity, then

$$\lim_{\gamma\to\infty} G = (1-\beta)\left(\frac{\alpha}{\beta}\right) \tag{2.7}$$

Equation 2.7 shows that as the modulator sensitivity increases, the circuit gain becomes independent of the nonlinear terms a_1 and a_2, so the greater the value of γ, the smaller the distortion products.

Lavrushenkov, Novikov, and Chugunov [9] reported up to a 35 dB reduction in distortion products using envelope feedback, but also found that the circuit is sensitive to operating conditions such as gain imbalance, gain uniformity over the bandwidth, power supply stability, and temperature stability.

2.3.4) Baseband Linearization

Also known as Cartesian Feedback [6], this technique is closely related to the predistortion and adaptive predistortion schemes, differing only in that it uses continuous feedback loop. Again, due to the delay inherent in the feedback loop, the amplifier suffers from stability problems and a narrow bandwidth.

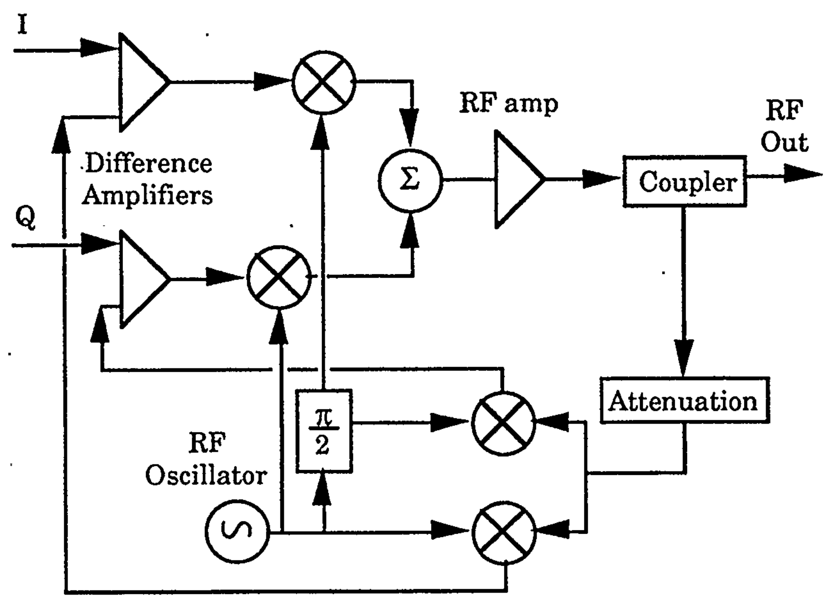

Figure 2.6 Cartesian Feedback Linearizer

The circuit schematic is shown in Figure 2.6 [6]. The amplifier output is first sampled using a coupler. Then the sampled signal is attenuated and coherently demodulated to recover the quadrature Cartesian components of the modulation signal. These signals are used to provide the negative feedback, being subtracted from the modulation I and Q channels at the amplifier's input to provide the loop error signal. If the loop gain is great enough, the feedback loop will correct for any nonlinearity in the up-conversion and RF amplification stages. Although the figure illustrates an analog system, Cartesian feedback has been principally realized using DSP techniques for the generation of the error signal.

Two techniques have been proposed to eliminate the stability problems caused by the phase delay in the amplifier. The first is a software controlled phase shift in the demodulation oscillator which would minimize the phase error in the feedback signals. The second is to digitize the feedback signals and to calculate and correct for the phase errors using DSP software.

Reduction of the intermodulation products achieved for a two tone test using this technique have been reported as high as 30 dB [6].

2.4) Predistortion Linearization

Predistortion and feedforward linearization techniques are closely related. Both use signal cancellation to remove the unwanted distortion in the output signal, but while feedforward splits, processes, and recombines the nonlinear amplifier output after amplification, predistortion modifies the amplifier's input signal only.

Predistortion can be applied to the baseband, IF, or RF stages of the radio. In all three cases the principle of operation is the same; a signal containing the inverse of the output amplifier's distortion products is added to the desired signal, which is upconverted if required and then fed to the nonlinear amplifier. During the amplification, the distortion products are canceled by the predistortion added earlier.

There are basically two techniques for generating the predistortion signal. A nonlinear analog device is used to generate a set of distortion products which are phased and added to the original signal [10][11], or adaptive DSP techniques are used to modify the IF [14] or baseband [12][13] signals. In order to demonstrate the principle, we will consider only the RF cuber and adaptive complex gain methods of predistortion. If the reader wishes to investigate IF predistortion please see references [1] and [14].

2.4.1) RF Cuber Predistortion

The cuber technique uses predistortion to compensate for the third order intermodulation distortion generated in the power amplifier, which is usually the largest of the distortion products. A reduction in distortion of more than 20 dB per 25 MHz bandwidth has been reported using this technique [10].

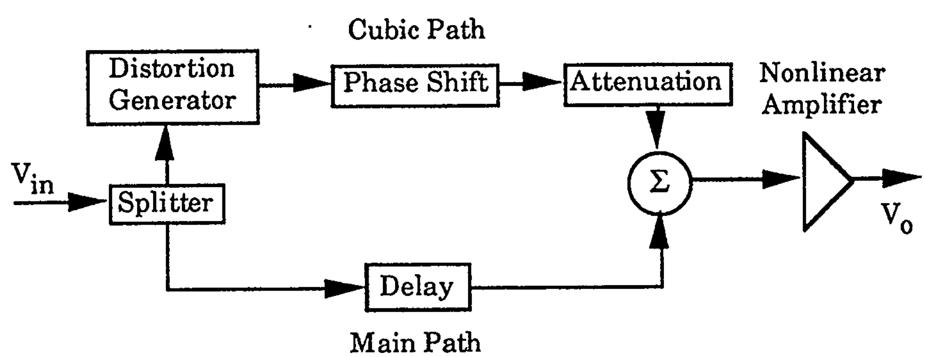

Figure 2.7 Basic Cuber Predistortion Linearizer

The fundamental CPL circuit configuration is shown in Figure 2.7 [10]. The required characteristics of the CPL are calculated by analyzing the distortion characteristics of the nonlinear amplifier. The generation of the distortion can be accomplished using either passive [10][11] or active components [1]. The phase and amplitude of the distortion signal are adjusted to the required values, and then the signal is added to a delayed version of the non distorted signal.

The CPL linearizer offers some improvement, but cannot compensate for temperature drift, component aging, and dc power variations. In order to achieve optimal performance the linearizer can be made self-adjusting. An adaptive cuber predistorter has been reported [10] that is realized by adding a separate training loop and computer control. The amplifier is isolated from the circuit through RF switches, and then fed two tones. The third order distortion products are detected and the predistortion circuitry adjusted in order to minimize the distortion. The training cycle is less than 5 ms in duration. The circuit achieved greater than 20 dB reduction in third order distortion products over temperature and bandwidth ranges.

2.4.2) Adaptive Complex Gain Predistortion

Adaptive complex predistortion is one of the most promising of the new linearization techniques. Several adaptive predistortion techniques have been reported, but most have been restricted in modulation scheme or order and type of PA nonlinearity. The first general technique was reported by Nagata [14] who, through a generalization of the adaptive QAM linearizer reported by Saleh and Salz [18], developed a method that was independent of modulation scheme or of the amplifier nonlinearity. Although Nagata was able to report -60 dBc out of band emissions for a 33% efficient amplifier, there were several problems in the circuit realization, including:

- A large lookup table, 20 MByte of RAM required.
- Slow convergence time for the adaptation and memory table update (approximately 10 sec).
- Phase shift adjustment and slow reconvergence if amplifier

input frequency was changed.

- A phase shifter was required in the feedback network for stability.

A solution to these realization problems has been proposed by Cavers [15] through the use of complex gain predistortion. By treating the amplifier distortion as a memoryless nonlinearity, Cavers has been able to reduce the look up table by four orders of magnitude, to typically less than 100 complex word pairs, eliminated the convergence and reconvergence problem, and eliminated the need for the phase shifter.

Cavers' work has been verified experimentally by Wright [16] and through simulation by den Otter [17]. The experimental system used by Wright is shown in Figure 2.8 [16].

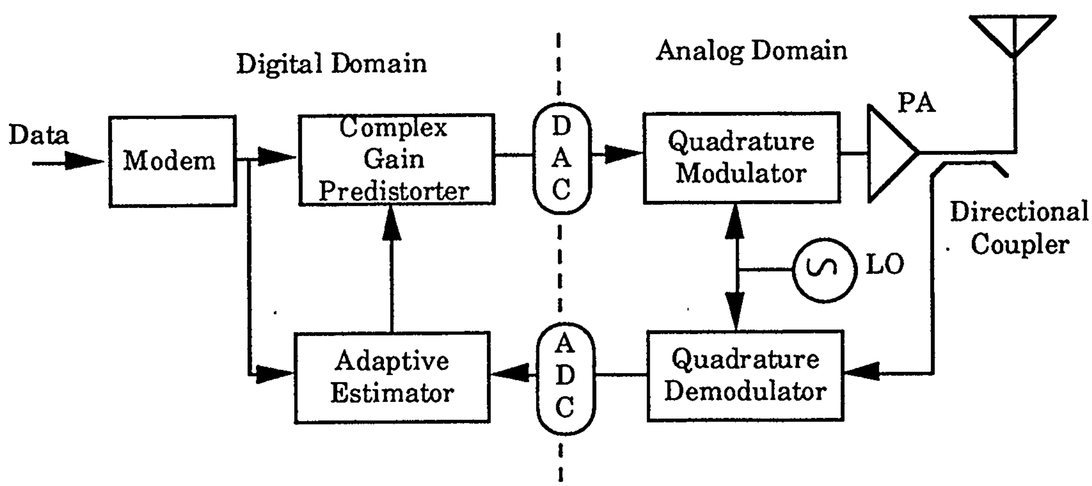

Figure 2.8 Adaptive Predistortion Linearization Circuit

While den Otter reported an adjacent channel power level reduction of better than -30 dB in her simulation, Wright was only able to achieve a -20 dB reduction. The difference in performance between the simulation and hardware was apparently due to the sensitivity of the predistortion to local oscillator feedthrough and gain/phase imbalance for the I and Q channels of the modulators and demodulators. den Otter also compared the complex gain predistorter and Cartesian feedback, finding that the predistorter gave the larger reduction close to the channel, while the Cartesian feedback gave a better reduction farther away from the channel.

2.5) Modified Feedback Amplifier

The reduction of the amplifier's intermodulation products is accomplished through the negative feedback of the intermodulation products only, with the fundamentals and their harmonics removed from the feedback loop. The effect of the negative feedback on the desired signal is reduced through this cancellation of the fundamentals. The block diagram illustrating the circuit performance is shown below in Figure 2.9. Note that the graphical representation of the IM products shown in the figure are derived from the open loop condition and would not necessarily be accurate for the closed loop condition.

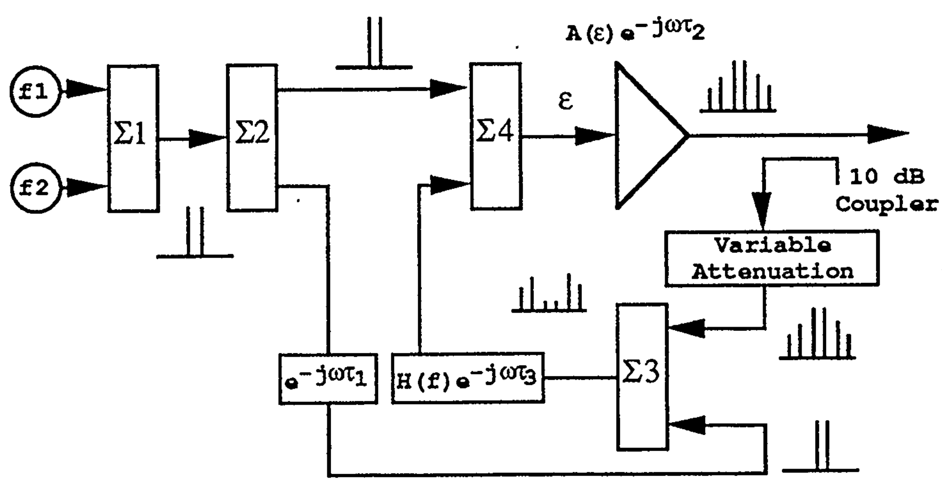

Figure 2.9 Experimental System Block Diagram

Two equal amplitude input tones are combined at the first summer

($\Sigma 1$) to provide a two tone test test signal, which is fed to the circuit. The test signal is then split ($\Sigma 2$) into two equal amplitude paths. The upper path is combined with the feedback signal ($\Sigma 4$) to form the error signal which is fed to the amplifier. The amplifier output signal, containing the harmonic and intermodulation distortion products, is sampled by a directional coupler, attenuated and then combined with the lower signal path ($\Sigma 3$).

The signal in the lower path is passed through a delay which is equal to the upper path delay, which consists of of the sum of the combiner, amplifier, and coupling delays, plus an additional delay equal to π radians at the center frequency. The additional delay can be eliminated if a 0° and 180° summer is used at $\Sigma 2$. The fundamental tones arriving at $\Sigma 3$ through the upper and lower paths are now of equal amplitude and are 180° out of phase at the center frequency. The summation causes cancellation of the fundamental tones, while the amplifier's harmonic and IM products contained in the upper path are only scaled in amplitude. For the case of the additional delay, complete cancellation occurs only at the center frequency, with the level of attenuation decreasing as the deviation from the center frequency increases. If the $0^\circ/180^\circ$ splitter is used, then the cancellation will occur over a larger bandwidth.

The output signal from $\Sigma 3$ is then bandpass filtered to remove the harmonic and out of band intermodulation products, scaled in amplitude and shifted in phase, which is represented in Figure 2.9 by H(f). The feedback signal is then combined with the upper path ($\Sigma 4$) to form the error signal. The cancellation of the fundamental in the feedback loop reduces the loop gain for the desired signal while leaving the distortion product loop gain unaffected.

Chapter Three

Nonlinear Amplifier Distortion

The ideal transfer function for a linear amplifier produces a scaled and delayed replica of the input signal, while nonlinear amplifier effects will produce distortion in the amplitude and phase characteristics of the output signal. These effects can be characterized by amplitude compression, generation of harmonic and intermodulation frequencies, group delay and phase distortion. The results of these nonlinearities are reduced system dynamic range, spectral growth through the intermodulation products, and signal distortion.

The model of a nonlinear amplifier depends on whether or not the circuit can be considered memoryless. If the amplifier is considered memoryless with a mild nonlinearity, then its amplitude transfer function can be represented by a power series. If the system has memory, then the amplifier may be more accurately represented by the Volterra series. In either case, most of the amplifier's distortion characteristics can be predicted once the series coefficients are known.

This section of the thesis deals with the types of distortions found in a nonlinear amplifier, and their prediction using a power series.

3.1) Memoryless Amplitude Distortion

An amplifier may be considered linear in its amplitude characteristic if the output power increases linearly with the input power. The ratio between the input and output power is defined as the amplifier gain G. For any practical amplifier, there exists a point at which the amplifier will begin to saturate, which results in an output power which is lower than that predicted by the linear gain, causing an amplitude distortion of the output signal. This distortion can be characterized by the 1 dB compression point, which is defined as that point at which the amplifier gain drops 1 dB below the linear gain, as shown in Figure 3.1.

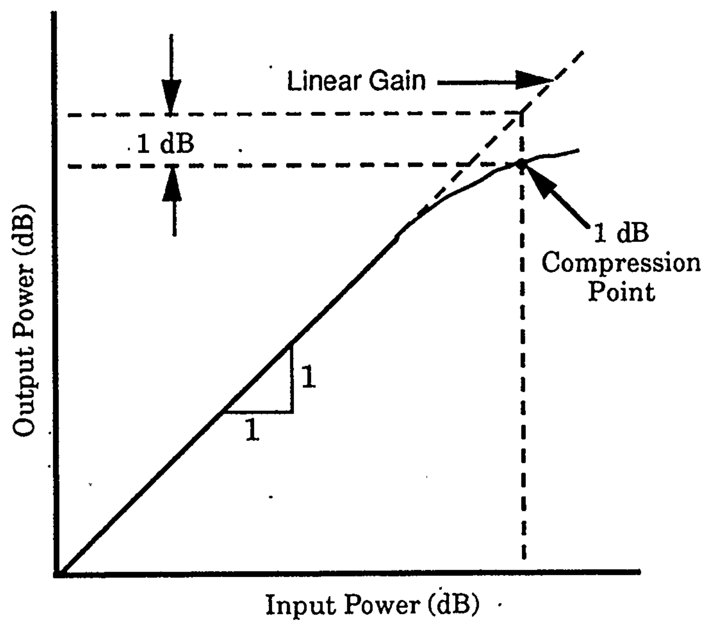

Figure 3.1 Nonlinear Amplitude Characteristic

If the amplifier nonlinearity is weak, then its output voltage can be represented by a short power series [18], such as

$$v_o(t) = k_1 v_i(t) + k_2 v_i^2(t) + k_3 v_i^3(t) \tag{3.1}$$

If we let $v_i = A\cos(w_1 t)$, then v_o can be written as

$$\begin{aligned} v_o(t) = {} & \frac{1}{2}k_1A^2 + \left(k_1A + \frac{3}{4}k_3A^3\right)\cos(\omega_1 t) + \frac{1}{2}k_2A^2\cos(2\omega_1 t) \\ & + \frac{1}{4}k_3A^3\cos(3\omega_1 t) \end{aligned} \tag{3.2}$$

This result shows that the output voltage waveform consists of the fundamental combined with a dc term and the second and third order harmonics of the input signal. Examination of Equation 3.2 shows that in order to represent a gain compressive system such as an amplifier, then k_3 must be less than zero.

This simple model can be used to estimate some of the performance characteristics of the amplifier. From Equation 3.2, the gain at the fundamental frequency can be written as

$$G = 20\log\left(\frac{k_1 A + \frac{3}{4}k_3 A^3}{A}\right) = 20\log\left(k_1 + \frac{3}{4}k_3 A^2\right) \tag{3.3}$$

which is dependent on the level of the input signal, unlike the linear gain $G_0 = 20\log(k_1)$. If we consider the 1 dB compression point, which was defined above as $G_{1dB} = G_o - 1$, then from Equation 3.3 we can write

$$k_1 + \frac{3}{4}k_3 A^2 = 0.89k_1 \tag{3.4}$$

From Equation 3.4, the input amplitude at the 1dB compression point is found to be

$$A = \sqrt{0.145\frac{k_1}{|k_3|}}, \quad k_3 < 0 \tag{3.5}$$

If it is assumed that the input impedance is R ohms, then the input power in dBm may be written as

$$P_i = 10\log\left\{\left(\frac{A}{\sqrt{2}}\right)^2 \frac{10^3}{R}\right\} \tag{3.6}$$

If we let R = 50 Ω, then Equation 3.6 can be written as

$$P_i = 20\log\{A\} + 10 \quad \text{dBm} \tag{3.7}$$

The output power at the 1 dB compression point can be written as

$$P_{1dB} = G_o - 1 + P_i \quad \text{dBm} \tag{3.8}$$

Substituting (3.5) and (3.6) into (3.8), and assuming that R = 50 ohms, then we can write the 1 dB compression point output power as

$$P_{1dB} = 10\log\left(\frac{k_1^3}{|k_3|}\right) + 0.62 \qquad \text{dBm} \tag{3.9}$$

The 1 dB compression point is used as a common amplifier specification by manufacturers and designers. Equation 3.9 yields a simple amplifier model from this specification by solving for k_3.

3.1.1) The Two Tone Test

A standard test for amplifier amplitude linearity is the two tone test. Two equal amplitude sinusoids at different frequencies are combined and applied to the amplifier input. The resulting output signal consists of the fundamental frequencies combined with a dc term and several spurious frequency products which result from the amplifier's nonlinearity. The spurious products are made up of harmonics of the fundamental frequencies as well as even and odd order intermodulation products. An even order intermodulation product is defined as a spurious frequency in which the sum of the coefficients of the fundamental tones add to an even number, such as $2f_1 - 2f_2$ or $f_1 + f_3$. An odd order intermodulation product is defined as a spurious frequency in which the coefficients of the fundamental frequencies add to an odd number, such as $2f_1 - f_2$, $3f_1 - 2f_2$, or $5f_2 - 4f_1$...

If the system bandwidth is less than an octave, then most of the spurious frequency products will fall outside the passband and can be filtered out. However, the odd order intermodulation frequencies, such as $2f_2 - f_1$ or $4f_1 - 3f_2$, usually fall within the system passband and will cause output signal distortion. The resulting input and output spectra for a third order model are shown in Figure 3.2.

Another standard measure of the level of distortion introduced by the amplifier is the third order intercept point. It is defined as the output power level at which the third order intermodulation frequency IM_3, at $2f_1 - f_2$, or $2f_2 - f_1$ is equal to the output power of the fundamental f_1. The IM_3 intercept point can never actually be achieved due to the saturation effects within the amplifier, but because it is independent of the input power it is a good measure of amplifier linearity. The intercept point is derived through the extrapolation of the small signal response of the amplifier as shown in Figure 3.3. Note that at low input power the slope of the fundamental is 1:1

while the slope of IM_3 is 3:1.

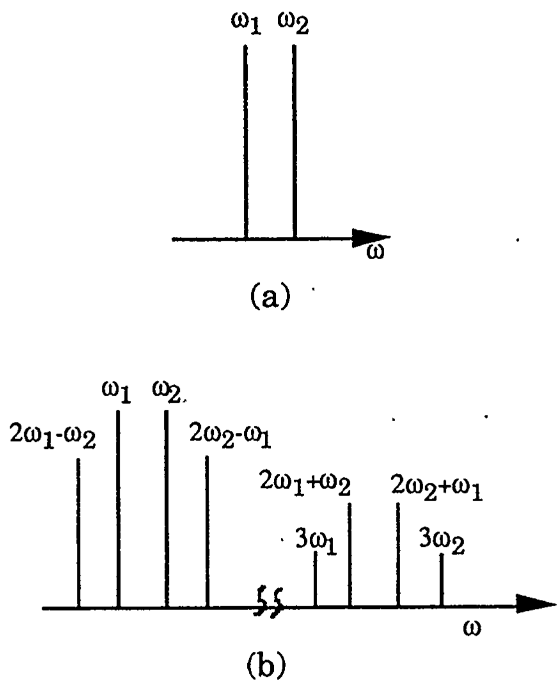

Figure 3.2 (a) Input Spectrum

(b) Third Order Model Ouput Spectrum

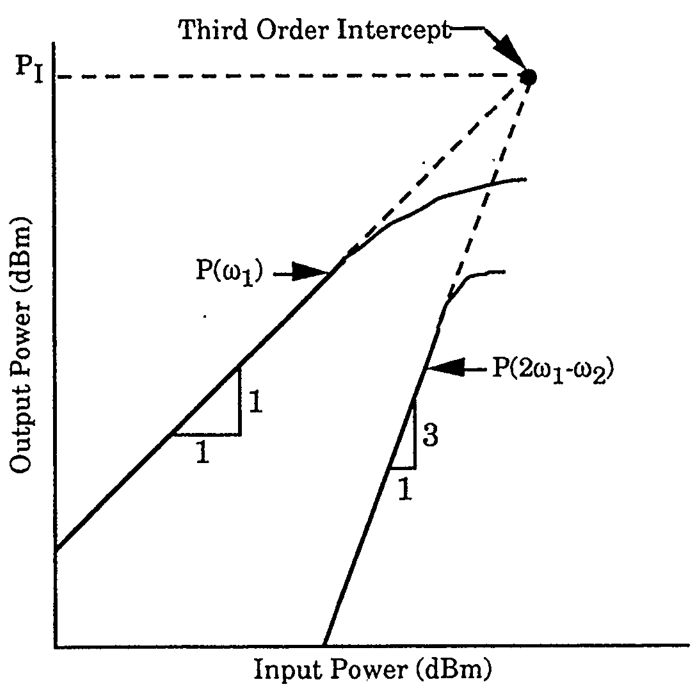

Figure 3.3 Definition of Third Order Intercept Point

The third order power series given in Equation 3.1 can also be used to estimate the amplifier performance in the two tone test. If we let $V_i(t) = A\{\cos(\omega_1 t) + \cos(\omega_2 t)\}$, substitution into equation 3.1 yields Equation 3.10, which represents the total output for a third order model,

$$\begin{aligned}
V_o(t) &= k_2A^2 + k_2A^2\cos(\omega_1-\omega_2)t + (k_1A + \frac{9}{4}k_3A^3)\cos(\omega_1 t) \\
&+(k_1A + \frac{9}{4}k_3A^3)\cos(\omega_2 t) + \frac{3}{4}k_3A^3\cos(2\omega_1-\omega_2)t \\
&+\frac{3}{4}k_3A^3\cos(2\omega_2-\omega_1)t + k_2A^2\cos(\omega_1+\omega_2)t + \frac{1}{2}k_2A^2\cos(2\omega_1 t) \\
&+\frac{1}{2}k_2A^2\cos(2\omega_2 t) + \frac{3}{4}k_3A^3\cos(2\omega_1+\omega_2)t + \frac{3}{4}k_3A^3\cos(2\omega_2+\omega_1)t \\
&+\frac{1}{4}k_3A^3\cos(3\omega_1 t) + \frac{1}{4}k_3A^3\cos(3\omega_2 t)
\end{aligned} \tag{3.10}$$

Assuming that the load is 50 ohms, then as was shown in Equation 3.6 we can write

$$P_{linear} = 20\log(k_1A) + 10 \text{ dBm} \tag{3.11}$$

$$P(\omega_1) = 20\log(k_1A + \frac{9}{4}k_3A^3) + 10 \text{ dBm} \tag{3.12}$$

$$P(2\omega_1 - \omega_2) = 20\log(\frac{3}{4}k_3A^3) + 10 \text{ dBm} \tag{3.13}$$

As equations 3.11 and 3.13 are equal at the IM_3 intercept point, we can write

$$k_1 A = \frac{3}{4} k_3 A^3$$

$$A^2 = \frac{4}{3} \frac{k_1}{|k_3|} \tag{3.14}$$

Substituting this result into Equation 3.11 yields

$$P_{\text{Intercept}} = 10\log\left(\frac{k_1^3}{|k_3|}\right) + 11.25 \text{ dBm} \tag{3.15}$$

Substituting Equation 3.9 into 3.15 results in

$$P_{\text{Intercept}} = P_{1\text{dB}} + 10.63 \text{ dBm} \tag{3.16}$$

Equation 3.16 is a useful result for mildly nonlinear amplifiers as the 1 dB compression point is an easily measured characteristic, but it will suffer an increasing error as the amplifier nonlinearity increases and the third order model becomes less accurate, and so should be treated as an approximation.

3.2) Group Delay

The nonlinear amplifier characteristics can also result in phase distortion. If the phase shift is linear over the passband of the system, then there is a constant time delay for all frequency components passing through the system. If the phase response is nonlinear, then the various frequency components of the signal will experience different degrees of time delay as they pass through the system, resulting in phase distortion.

The measure of the phase distortion due to the time delay is the group delay, which is defined as the negative of the derivative of the phase shift versus frequency.

$$t_d = -\frac{d\theta}{d\omega}$$

If the system has a linear phase characteristic, then t_d is a constant and no phase distortion results.

3.3) AM to PM Distortion

In addition to the phase distortion caused by a nonlinear phase response, further phase distortion can be introduced through AM-PM modulation. In this case the amplifier's phase characteristic is dependent on the instantaneous amplitude of the input signal.

Chapter Four
The Volterra Series

So far, the systems that have been discussed have been assumed to be memoryless, that is the system output is an instantaneous function of the input signal. However, there is a second class of systems in which the system output is a function of both the present and past values of the input signal. These systems are considered to have a memory.

The power series used earlier can give an adequate model of the system response for a weak memoryless nonlinearity, but is limited in two areas. First, the power series is dependent on the input signal, and as such cannot be considered a true transfer function. Secondly, the power series cannot model a system with memory. This presents a serious limitation as the components of most communication systems can be considered to possess memory to some extent. It is possible to overcome this limitation though through an extension of the power series called the Volterra series, which is used in the nonlinear transform function approach.

This section discusses the Volterra series, and considers the nonlinear transfer function concept and its application to multitone measurements such as the two tone test discussed earlier.

4.1) The Volterra Functional Series

The nonlinear transfer function approach models the response of a weakly nonlinear system as a sum of N individual responses, as is shown in Figure 4.1 [24]. The model consists of the parallel combination of N blocks, all of which share a common input x(t). The total response is obtained by summing the outputs of the blocks yielding y(t).

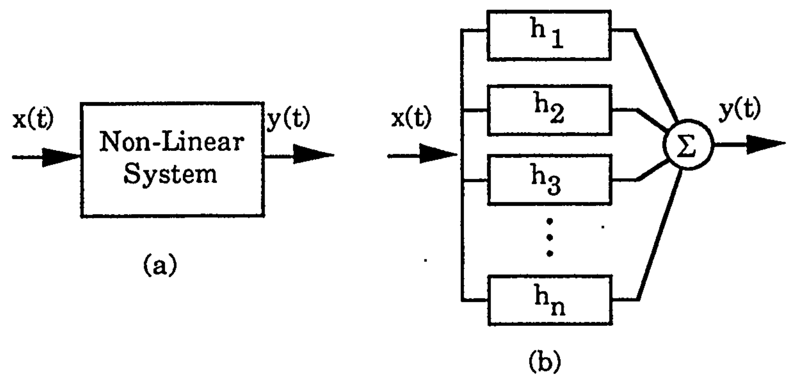

Figure 4.1 (a) Nonlinear System

(b) Functional Expansion of a Nonlinear System

The nth order block, which is characterized by the nth order transfer function, is of the order n in that if the input x(t) is multiplied by A, then the output of the block will be multiplied by A^n. This does not correspond to the degree of a power series, which refers to the highest exponent used in the polynomial. This is illustrated by the fact that the order of the ouput of a power series is limited to the degree of the polynomial used, while the degree of the output of an nth order nonlinear transfer function can be greater than the block's order.

The transfer functions shown above in Figure 4.1 are known as the nonlinear system's Volterra series kernels.

The use of the Volterra series can be considered as a generalization of the convolution integral which is used in linear system analysis. The linear portion of the system response is characterized by the first order kernel h_1, the quadratic portion of the response is characterized by the second order kernel h_2, and so on until the number of terms is sufficient to represent y(t).

It has been shown by Parente [19] that for any time invariant deterministic system S, there exists a functional F such that, for all real t and each <x,y> $\in$ S,

$$y(t) = F[x(t-u)]_{u=a}^{b}$$

where x is the input to the system, y is the system output, and the system S is either linear or nonlinear in nature. The interval (a,b) is called the memory of the system, where if a = b = 0, then the system is memoryless, or if a = b > 0, then the system is a pure delay. S is realizable if a >= 0, but if a < 0 the system is non-causal and is non-realizable.

If the nonlinear system S is continuous [21], then it may be represented by a functional power series, also known as the Volterra series, as is shown by Ha [18]:

$$\begin{aligned} y(t) = \sum_{n=1}^{\infty} y_n(t) = &\int_{-\infty}^{\infty} h_1(u_1)x(t-u_1)du_1 \\ &+ \int_{-\infty}^{\infty}\int_{-\infty}^{\infty} h_2(u_1,u_2)x(t-u_1)x(t-u_2)du_1du_2 \\ &+ \int_{-\infty}^{\infty}\int_{-\infty}^{\infty}\int_{-\infty}^{\infty} h_3(u_1,u_2,u_3)x(t-u_1)x(t-u_2)x(t-u_3)du_1du_2du_3 + \ldots \end{aligned} \tag{4.1}$$

where

$$y_n(t) = \int_{-\infty}^{\infty}\cdots\int h_n(u_1,u_2,\ldots,u_n)x(t-u_1)x(t-u_2)\ldots x(t-u_n)du_1du_2\ldots du_n \tag{4.2}$$

The function h_n in the functional power series is called the nth kernel of the Volterra series H, and the term it appears in is called the nth order functional of H. It can be seen that the first term of Equation 4.1 is simply the convolution of the impulse response of a linear network, and that the series is an extension of the convolution integral used in linear system analysis.

The kernels of the Volterra series are not unique in that interchanging the order of the arguments of $h_n(u_1,u_2,\ldots,u_n)$ does not effect the output of the kernel. However, a unique kernel can be obtained through an operation known as the symmetrization of h_n, where Sym is defined as

$$\mathrm{Sym}\{h_n\} = \frac{1}{n!} \sum_{\begin{bmatrix}\text{all permutations}\\ \text{of } u1,u2,\ldots,u3\end{bmatrix}} h_n(u_1,u_2,\ldots,u_n)$$

$$= h_n'(u_1,u_2,\ldots,u_n) \tag{4.3}$$

Sym $\{h_n\}$ is the sum of the values of h_n , which has been evaluated at all n! permutations of the arguments, divided by n!. Any kernel h_n can be replaced by its symmetrization without altering the output.

An n dimensional Fourier transform of the nth order impulse response can be taken, as shown in Equation 4.4, which yields the nth order nonlinear transfer function as

$$H_n(\omega_1,\omega_2,\ldots,\omega_n) = \int_{-\infty}^{\infty}\cdots\int h_n(u_1,u_2,\ldots,u_n)\exp[-j(\omega_1 u_1$$

$$+\omega_2 u_2+\ldots+\omega_n u_n)]du_1 du_2\ldots du_n \tag{4.4}$$

Conversely, an inverse transfer function can be defined as

$$h_n(u_1, u_2, \ldots, u_n) = \int_{-\infty}^{\infty} \cdots \int H_n(\omega_1, \omega_2, \ldots, \omega_n) \exp[j(\omega_1 u_1 + \omega_2 u_2 + \ldots + \omega_n u_n)] d\omega_1 d\omega_2 \ldots d\omega_n \tag{4.5}$$

Note that, as in the case of the nth order kernel, the transfer function H_n is not unique in that several nth order kernels may give the same nth order output y_n for the same input x_n, again due to the fact that interchanging the order of the arguments of $h_n(u_1, u_2, \ldots, u_n)$ does not affect the output. Hence the transfer function can also be symmetrized as

$$H'_n(\omega_1, \omega_2, \ldots, \omega_n) = \frac{1}{n!} \sum_{\left[\substack{\text{all permutations} \\ \text{of } \omega 1, \omega 2, \ldots, \omega 3}\right]} H_n(\omega_1, \omega_2, \ldots, \omega_n) \tag{4.6}$$

Substitution of the nth inverse transfer function, as given in Equation 4.5, into the nonlinear transfer function given in Equation 4.2 yields

$$y_n(t) = \int_{-\infty}^{\infty} \cdots \int H_n(\omega_1, \omega_2, \ldots, \omega_n) \prod_{i=1}^{n} X(\omega_i) \exp(j\omega_i t) d\omega_i \tag{4.7}$$

where $X(\omega_i)$ is the Fourier transform of $x(t)$ with frequency ω_i. Taking the Fourier transform of Equation 4.7 yields

$$Y_n(\omega) = \int_{-\infty}^{\infty} \cdots \int H_n(\omega_1, \omega_2, \ldots, \omega_n) \delta(\omega - \omega_1 - \omega_2 - \ldots - \omega_n) \prod_{i=1}^{n} X(\omega_i) d\omega_i \tag{4.8}$$

Now the frequency domain version of the functional power series as shown in Equation 4.1 can be written as

$$Y(\omega) = \sum_{n=1}^{\infty} Y_n(\omega) \tag{4.9}$$

4.1.2) Nonlinear Transfer Functions

Although it is clear that a weakly nonlinear system can be represented by the Volterra series, the problem of how to determine a given system's nonlinear transfer functions remains. Ha [18] has shown that, given the system equations are known and the system's transfer functions can be represented by a Volterra series, a system's nonlinear transfer functions can be found through the harmonic input method.

The harmonic input method is based on the fact that for a Volterra series a harmonic input must result in a harmonic output. If we let the input be a sum of k exponentials

$$x(t) = \sum_{k=1}^{K} A_k \exp(j\omega_k t) \tag{4.10}$$

where A_k can be complex and ω_k can be any positive or negative real number. Substitution of Equation 4.10 into the expression given for the nth order Volterra kernel given in Equation 4.2 yields

$$\begin{aligned} y_n(t) &= \int_{-\infty}^{\infty} .. \int h_n(u_1, u_2, \ldots, u_n) \prod_{i=1}^{n} \sum_{k=1}^{K} A_k \exp[j\omega_k (t - u_i)] du_i \\ &= \sum_{k_1=1}^{K} \cdots \sum_{k_n=1}^{K} \prod_{i=1}^{n} A_k \exp(j\omega_{k_i} t) \int_{-\infty}^{\infty} .. \int h_n(u_1, u_2, \ldots, u_n) \prod_{i=1}^{n} \exp(j\omega_k u_i) du_i \end{aligned} \tag{4.11}$$

The second half of Equation 4.11 can be seen to be the Fourier transform of the nth order impulse response as was given in Equation 4.4. Substitution of Equation 4.4 into Equation 4.11 yields Equation 4.12 in which Hn is a complex constant dependent on the defined input frequencies.

(4.12)

$$y_n(t) = \sum_{k_1=1}^{K} \sum_{k_2=1}^{K} \cdots \sum_{k_n=1}^{K} \left[\prod_{i=1}^{n} A_{k_i} \exp(j\omega_k t) \right] H_n(j\omega_{k_1}, j\omega_{k_2}, \ldots, j\omega_{k_n})$$

$$= \sum_{k_1=1}^{K} \sum_{k_2=1}^{K} \cdots \sum_{k_n=1}^{K} \left[\left(\prod_{i=1}^{n} A_{k_i} \right) H_n(j\omega_{k_1}, \ldots, j\omega_{k_n}) \exp[j(\omega_{k_1} t + \ldots + \omega_{k_n} t)] \right]$$

This result can be used to develop the nonlinear transfer function for any order n and number of inputs k. As an example, consider the case for two input exponentials (k=2) with the desired kernel being $y_2(t)$. In this case the input becomes $x(t)=A_1\exp(j\omega_1 t)+A_2\exp(j\omega_2 t)$. Using Equation 4.12 yield

(4.13)

$$y_2(t) = \sum_{k_1=1}^{2} \sum_{k_2=1}^{2} A_{k_1} A_{k_2} H_2(j\omega_{k_1}, j\omega_{k_2}) \exp[j(\omega_{k_1} + \omega_{k_2})t]$$

$$= A_1 A_1 H_2(j\omega_1, j\omega_1) \exp(j2\omega_1 t) + A_1 A_2 H_2(j\omega_1, j\omega_2) \exp[j(\omega_1 + \omega_2)t]$$

$$+ A_2 A_1 H_2(j\omega_2, j\omega_1) \exp[j(\omega_2 + \omega_1)t] + A_2 A_2 H_2(j\omega_2, j\omega_2) \exp(j2\omega_2 t)$$

4.1.3) Two Tone Measurement

Now that expressions have been derived for the nonlinear transfer functions in terms of the Volterra kernels, the remaining problem is to relate these results to measurable circuit parameters. This will be accomplished by first considering the nonlinear transfer function response to a multitone input, and then the specific response for the two tone case which corresponds to the two tone test discussed earlier.

Consideration of Equation 4.12 shows that for any given output frequency, $y_n(t)$ contains n! terms at that frequency, each of which corresponds to a permutation of the argument of the exponential $\omega_1 + \omega_2 + \ldots + \omega_n$. Ha [18] has shown that the output will contain no other terms at this frequency other than those in $y_n(t)$ if the input frequencies are linearly independent, that is, there is no set of rational numbers such that

$$\sum_{i=1}^{n} m_i \omega_i = 0 \tag{4.14}$$

where not all of m can be equal to zero.

Further examination of equation 4.12 shows that any of the possible output frequencies, $\omega_o = \omega_1 + \omega_2 + \ldots + \omega_n$, can be represented as $m_1\omega_1 + m_2\omega_2 + \ldots + m_k\omega_k$, where m_i , i = 1, 2, ..., k, are non-negative integers. If $m_1 + m_2 + \ldots + m_k = n$, then $\omega_o = m_1\omega_1 + m_2\omega_2 + \ldots + m_k\omega_k$ is the frequency output of the nth order nonlinear transfer function.

If the nth order transfer function is symmetrized, and if the input frequencies are linearly independent, then the sum of all the terms containing the frequency $\omega_o = m_1\omega_1 + m_2\omega_2 + \ldots + m_k\omega_k$ for the nth nonlinear transfer function is given by

$$y_{\omega_o}(t) = n!\left[\prod_{k=1}^{K} \frac{A_k^{m_k}}{m_k!}\right] H_n\left(m_1[j\omega_1], m_2[j\omega_2], \ldots, m_k[j\omega_k]\right) \exp(j\omega_o t) \tag{4.15}$$

where $\quad \sum_{k=1}^{K} m_k = n \quad$ and $\quad m_i[j\omega_i] = \overbrace{(j\omega_i, j\omega_i, \ldots, j\omega_i)}^{i \text{ times}}$

Now if we consider a K tone real input signal, x(t)

$$
\begin{aligned}
x(t) &= \sum_{k=1}^{K} |A_k| \cos(\omega_k t + \angle A_k) \\
&= \sum_{k=1}^{K} \left[\frac{A_k}{2} \exp(j\omega_k t) + \frac{A_k^*}{2} \exp(-j\omega_k t) \right]
\end{aligned}
\tag{4.16}
$$

If we denote $A_{-k} = A_k^*$, and $\omega_{-k} = -\omega_k$ then Equation 4.16 can be written as

$$
x(t) = \sum_{\substack{k=-K \\ k \neq 0}}^{K} \frac{A_k}{2} \exp(j\omega_k t) \tag{4.17}
$$

then Equation 4.15 can be rewritten as

$$
y_{\omega_o}(t) = n! \left[\prod_{\substack{k=-K \\ k \neq 0}}^{K} \frac{(A_k / 2)^{m_k}}{m_k!} \right] H_n\left(m_{-k}[j\omega_{-k}], \ldots, m_{-1}[j\omega_{-1}], \ldots, m_k[j\omega_k]\right) \exp(j\omega_o t) \tag{4.18}
$$

Equation 4.18 can be used to find the nonlinear transfer function for any value of n. As an example, consider one of the third order nonlinear transfer functions for a two tone input, at the fundamental frequency ω_1, which would be written as $H_3(-j\omega_1, j\omega_1, j\omega_1)$.

The system input would be written as

$$x(t)=\sum_{\substack{k=-2\\k\neq 0}}^{2}\frac{A_k}{2}\exp(j\omega_k t)$$

Applying Equation 3.34 with n=3, K=2, and m=[0, 1, 2, 0] where ω_o=[$m_1(-\omega_2)$, $m_2(-\omega_1)$, $m_3(\omega_1)$, $m_4(\omega_2)$], yields

$$y_3(\omega_1)=3!\left[\prod_{\substack{k=-2\\k\neq 0}}^{2}\frac{(A_k/2)^{m_k}}{m_k!}\right]H_n(-j\omega_1,j\omega_1,j\omega_1)\exp(j\omega_1 t)$$

$$=6\left[\frac{A_1}{2}\right]\left[\frac{|A_1/2|^2}{2!}\right]H_3(-j\omega_1,j\omega_1,j\omega_1)\exp(j\omega_1 t)$$

$$=\frac{3}{8}|A_1|^2A_1H_3(-j\omega_1,j\omega_1,j\omega_1)\exp(j\omega_1 t)$$

Using this procedure, Ha has shown that for a two tone input and a third order nonlinear transfer function, the outputs for the fundamentals and the third order intermodulation frequency can be written as

$$y_{(\omega_1)}(t)=|B_1|\cos(\omega_1 t+\angle B_1) \tag{4.19}$$

$$y_{(2\omega_1-\omega_2)}(t)=|B_2|\cos\left((2\omega_1-\omega_2)t+\angle B_2\right) \tag{4.20}$$

where

$$B_1=A_1H_1(j\omega_1)+\frac{3}{4}A_1^2A_1H_3(-j\omega_1,j\omega_1,j\omega_1)+\frac{3}{2}|A_2|^2A_1H_3(-j\omega_2,j\omega_1,j\omega_2)$$

and $$B_2 = \frac{3}{4} A_1^2 A_2^* H_3(j\omega_1, j\omega_1, -j\omega_2)$$

Although there is some similarity between Equations 4.19 and 4.20, and Equation 3.9 which was developed earlier from the power series representation, the nonlinear transfer functions are different in that they are independent of the input function. These equations will be used as a part of the experiment in order to determine the first and third order Volterra kernels of the amplifier used.

4.2) Volterra Series Feedback Amplifier Analysis

The analysis of a feedback loop containing a nonlinear element cannot make use of linear techniques. Through the Volterra series representation of the nonlinear amplifier, the circuit can be successfully analyzed with the standard linear control theory techniques. This section of the thesis deals with the analysis of the feedback amplifier using the Volterra series representation, and the derivation of the nonlinear transfer functions for the overall feedback circuit. These equations will be used in the prediction of the performance of the proposed modified feedback circuit.

4.2.1) Nonlinear Distortion Feedback Effects

The negative feedback amplifier circuit can be represented as a feedback control system such as those used in linear system control, as shown in Figure 4.2.

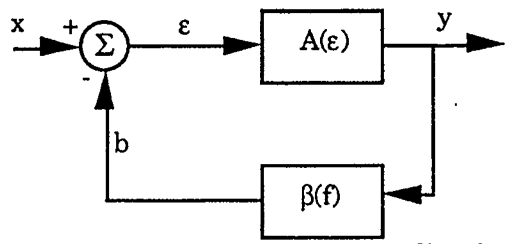

Figure 4.2 Nonlinear Feedback Control System

Narayanan [20] has shown that if the nonlinear amplifier, A(ε), is represented in a functional expansion by the first three of its Volterra kernels, and if linear and frequency dependent feedback is assumed, then expressions can be derived for the overall feedback amplifier circuit's nonlinear transfer function in terms of the open loop kernels and the feedback network as shown below in Figure 4.3 [20].

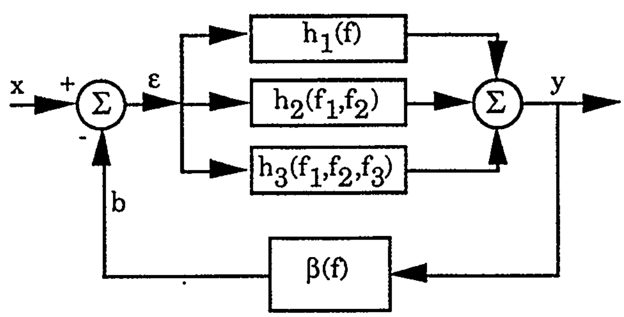

(a)

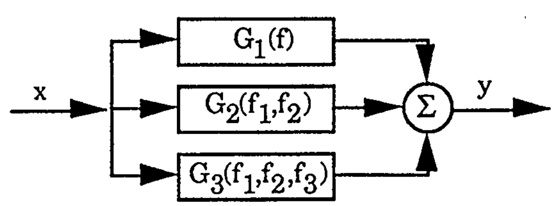

(b)

Figure 4.3 (a) Functional Expansion - Nonlinear System with Feedback
(b) Volterra Kernel Representation of (a)

The relationships in Figures 4.2 and 4.3 (a) can be written as

$$y = A(\varepsilon) \qquad y = G(x) \qquad \varepsilon = x - b \qquad b = \beta(y)$$

where $A(\varepsilon)$, $\beta(y)$, and $G(x)$ are the operators corresponding to the open loop amplifier, the feedback network, and the closed loop amplifier respectively. If the variables y, b, and ε are eliminated from the system as is shown in Figure 4.3 b, then the system equation can be written as

$$G(x) = h[x - \beta(G(x))] \tag{4.21}$$

If Equation 4.21 is expanded in terms of the closed loop Volterra kernels, and the first, second, and third order terms equated, then expressions for the closed loop Volterra kernels can be derived [20]. The first order linear terms yield

$$G_1(f) = h_1(f)\left[1 - \beta_1(f)G_1(f)\right] \tag{4.22}$$

or

$$G_1(f) = \frac{h_1(f)}{1+\beta_1(f)h_1(f)} \tag{4.23}$$

which is simply the linear equation demonstrating that feedback reduces the linear gain $h_1(f)$ by the loop gain. Equating the second degree terms results in

$$G_2(f_1,f_2) = \frac{h_2(f_1,f_2)\prod_{i=1}^{2}\left(1-\beta_i(f_i)G_1(f_i)\right)}{1+\beta_1(f_1+f_2)h_1(f_1+f_2)} \tag{4.24}$$

Substitution for G_1 in Equation 4.24 yields

$$G_2(f_1,f_2)=\frac{h_2(f_1,f_2)}{[1+\beta_1(f_1)h_1(f_1)][1+\beta_1(f_2)h_1(f_2)][1+\beta_1(f_1+f_2)h_1(f_1+f_2)]} \tag{4.25}$$

Equation 4.25 shows that the reduction of the second order distortion products is not only due to feedback of the product frequencies $f_1 + f_2$, but is also dependent on the feedback of the fundamental frequencies f_1 and f_2.

The second order distortion products do not have a serious effect on the amplifier linearity performance as they usually fall outside the system passband. Of greater concern is the third order distortion products which produce the inband intermodulation terms. The effect of feedback on the third order products can be examined through equating the third order terms in Equation 4.21, resulting in

$$\begin{aligned} G_3(f_1,f_2,f_3)=\Bigg[&h_3(f_1,f_2,f_3)\prod_{i=1}^{3}\frac{1}{1+\beta_1(f_i)h_1(f_i)} \\ &-2h_2(f_1,f_2+f_3)\frac{1}{1+\beta_1(f_1)h_1(f_1)}\beta_1(f_2+f_3)G_2(f_2,f_3)\Bigg] \\ &\bullet\left(\frac{1}{1+\beta_1(f_1+f_2+f_3)h_1(f_1+f_2+f_3)}\right) \end{aligned} \tag{4.26}$$

Substitution for G_2 in Equation 4.26 yields Equation 4.27, which shows that the third order open loop amplifier distortion is reduced through a complex interaction of fundamental, second order, and third order products. The first part of the equation shows that the third order distortion is reduced by both the feedback of both the fundamental frequencies and the third order product frequencies (ie. $f_1 + f_2 + f_3$). The second term is the result of a second order feedback term being combined with a first order input and then being acted on by a second order kernel, $h_2(f_1, f_2+f_3)$. This term is reduced by the feedback at the fundamental, second order, and third order products, and is also effected by the second order feedback $\beta_1(f_2+f_3)$.

(4.27)

$$G_3(f_1,f_2,f_3) = \Bigg[h_3(f_1,f_2,f_3)\prod_{i=1}^{3}\frac{1}{1+\beta_1(f_i)h_1(f_i)}$$

$$-2h_2(f_1,f_2+f_3)\frac{1}{1+\beta_1(f_1)h_1(f_1)}$$

$$\bullet\left(\beta_1(f_2+f_3)h_2(f_2,f_3)\frac{1}{1+\beta_1(f_2)h_1(f_2)}\frac{1}{1+\beta_1(f_3)h_1(f_3)}\right)$$

$$\bullet\left(\frac{1}{1+\beta_1(f_2+f_3)h_1(f_2+f_3)}\right)\Bigg]\left(\frac{1}{1+\beta_1(f_1+f_2+f_3)h_1(f_1+f_2+f_3)}\right)$$

4.3) Proposed Modified Feedback

Examination of Equation 4.27 shows that if $|h_2| << |h_3|$, then the second order effects in G_3 can be neglected. As this is a realistic assumption for a mildly nonlinear amplifier, then Equation 4.27 can be written as

$$G_3(f_1,f_2,f_3) = h_3(f_1,f_2,f_3)\prod_{i=1}^{3}\frac{1}{1+\beta_1(f_i)h_1(f_i)}$$

(4.28)

$$\bullet\frac{1}{1+\beta_1(f_1+f_2+f_3)h_1(f_1+f_2+f_3)}$$

If Equation 4.28 is considered with respect to the lower third order intermodulation product of a nonlinear amplifier at $2f_1$-f_2, then Equation 4.28 yields

$$G_3(f_1,f_1,-f_2)=\frac{h_3(2f_1-f_2)}{1+\beta_1(f_1)h_1(f_1)}\bullet\frac{1}{1+\beta_1(f_1)h_1(f_1)}\bullet\frac{1}{1+\beta_1(f_2)h_1(f_2)}\bullet\frac{1}{1+\beta_1(2f_1-f_2)h_1(2f_1-f_2)} \tag{4.29}$$

Equation 4.29 shows that the reduction of the third order intermodulation products is dependent on both the loop gain for the fundamental input frequencies and the loop gain for the third order intermodulation product itself. Examination of Equations 4.23 and 4.29 together suggest that it is possible to achieve a reduction of the IM_3 product, without affecting the circuit gain for the fundamentals, if the loop gain for the fundamentals is made small. This would greatly reduce or eliminate the effect of the negative feedback on the circuit gain for the desired signal, while still supplying some level of reduction of the intermodulation products. This idea has been tested through experimentation, the details of which are given in the next section.

Chapter Five

Modified Feedback Circuit Design and Analysis

In order to test whether or not the distortion products can be reduced without affecting the circuit gain for the input signal, it is necessary to design a negative feedback amplifier that can allow independent control of the loop gain of the fundamentals. It was decided that the control of the fundamental levels would be best implemented through the cancellation of the fundamental signal by combining the input and output signals with the required amplitude and phase adjustments at a combiner within the feedback loop. The resulting circuit was discussed in Section 2.5, with the block diagram shown in Figure 2.9, which is repeated here as Figure 5.1 for the reader's convenience.

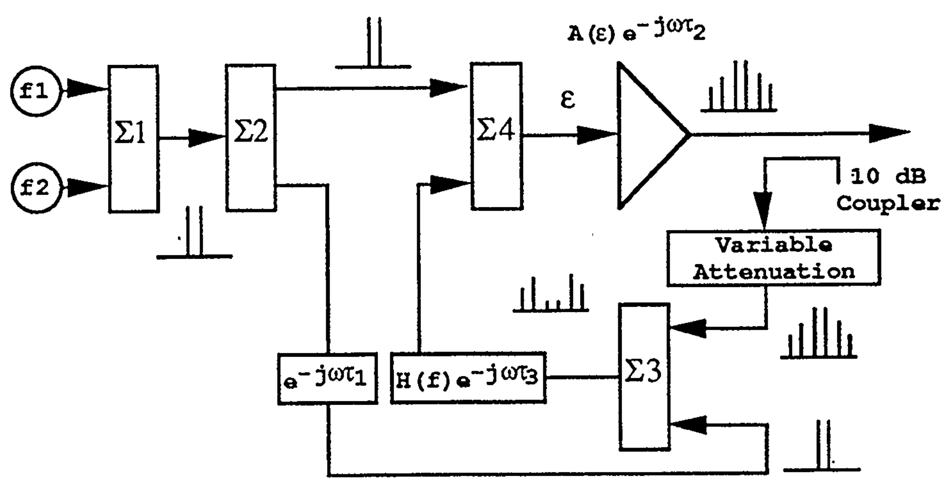

Figure 5.1 Experimental System Block Diagram

This section deals with the analysis of the circuit shown in Figure 5.1. The principle concern is with those areas which are responsible for limitations in the circuit performance, such as cancellation of the fundamental signal in the feedback loop and its effect on bandwidth, and a linear system model which leads to a stability and performance analysis of the closed loop system.

The results will show that the useable bandwidth of the circuit depends directly on the delay inherent in the amplifier being linearized, and that the amount of distortion reduction possible is directly dependent on both the amount of total circuit delay and the characteristic of the bandpass filter used as the loop filter in the feedback loop.

5.1) Circuit Analysis

This section deals with the analysis of the circuit's effective bandwidth and stability performance. The analysis shows that the useable bandwidth is directly dependent on the level of cancellation of the input signal at the cancellation node ($\Sigma 3$). The circuit stability is analyzed using linear control system methods and applying the Nyquist criteria.

5.1.1) Signal Cancellation

The level of cancellation of the input signal at the summing node $\Sigma 3$ is cricitcal because it determines the feedback loop gain for the input signals, which in turn affects the overall circuit gain, with greater levels of cancellation resulting in a greatly reduced loop gain for the input signal.

The problem of predicting the level of cancellation of the fundamentals at the summing node ($\Sigma 3$) can be reduced to that of the sum of two equal amplitude sinusoids, with the same frequency, arbitrary phase difference, and different delays. This is shown in Equation 5.1, with the starting phases arbitrarily set to zero

$$V_o(t) = \cos(\omega_o t - \omega_o \tau_1) + \cos(\omega_o t - \omega_o \tau_2) \tag{5.1}$$

If we declare that τ_2 is greater than τ_1, then τ_2 can be written as

$$\tau_2 = \tau_1 + \tau_\delta \qquad \text{where} \quad \tau_\delta > 0 \tag{5.2}$$

Substitution of Equation 5.2 into Equation 5.1 and using an algebraic identity yields

$$V_o(t) = 2\cos(\omega_o t - \omega_o \tau_1 - \frac{\omega_o \tau_\delta}{2})\cos(\frac{\omega_o \tau_\delta}{2}) \tag{5.3}$$

Equation 5.3 shows the output from the combiner to be a phase shifted version of the original signal multiplied by an attenuation factor, which can be considered as a sinusoidal envelope in the frequency domain, the characteristics of which are determined by the fixed relative delay τ_δ. The envelope magnitude goes to zero when the argument of the second cosine term in Equation 5.3 is some integer multiple of $\pi/2$. The magnitude of the envelope can be represented as

$$|V_o| = \left|2\cos\left(\frac{\omega_o \tau_\delta}{2}\right)\right| \tag{5.4}$$

This envelope produces nulls at regularly spaced intervals in the frequency domain for each value of τ_δ. Equation 5.4 shows that with increasing relative delay the frequency spacing between the nulls becomes smaller and the bandwidth of the nulls becomes narrower. If we define cancellation bandwidth as the frequency span, centered at a given null, over which the attenuation of the signal is equal to or greater than a given value, then it can be seen that the cancellation bandwidth decreases with increasing relative delay. This effect is shown below in Figure 5.2, which plots the cancellation bandwidth for differences in phase of $\omega\tau_\delta = n\pi$ radians for n=1, 3, and 5, at a normalized center frequency.

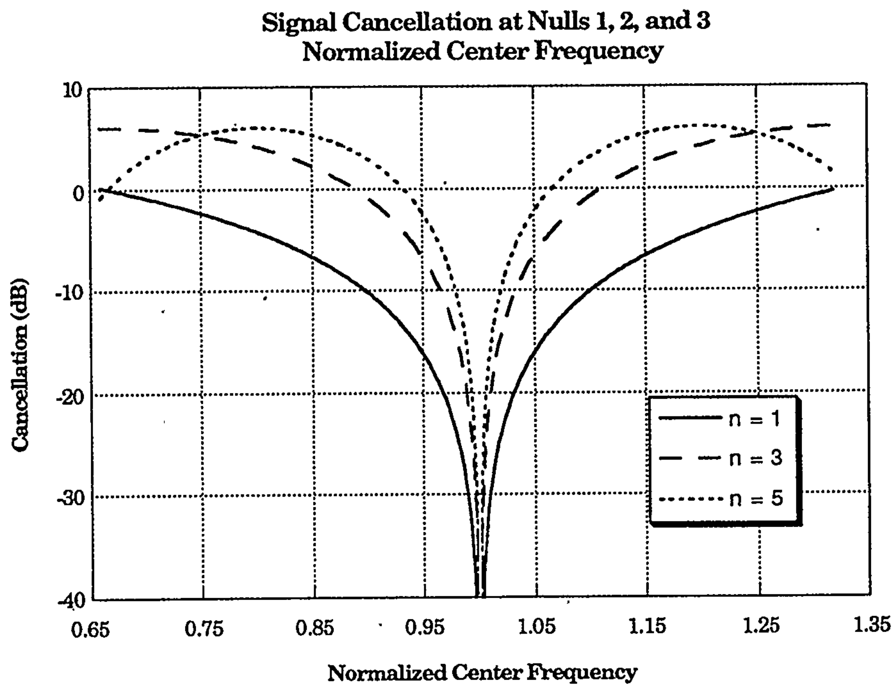

Figure 5.2. Predicted Attenuation at Cancellation Nulls 1, 2, and 3

In order to predict the level of cancellation, we first rewrite the argument of Equation 5.4 as

$$\frac{\omega\tau_\delta}{2} = n\frac{\pi}{2}\frac{f}{f_o} \tag{5.5}$$

where τ_δ is found to be $\tau_\delta = \frac{n}{2f_o}$.

The level of attenuation for a given normalized frequency relative to the unattenuated signal is found from Equation 5.6.

$$\text{Attenuation} = 20\log\left(\left|2\cos\left(n\frac{\pi}{2}\frac{f}{f_o}\right)\right|\right) \tag{5.6}$$

Equation 5.6 allows an estimation of the cancellation bandwidth if it is assumed that the cancellation envelope is symmetrical about f_o. A common definition for % bandwidth is

$$BW = \frac{f_{upper} - f_{lower}}{f_o} \tag{5.7}$$

Assuming symmetry about f_o, Equation 5.7 can be written as

$$BW = \frac{2(f_o - f_{lower})}{f_o}$$

or

$$\frac{f}{f_o} = 1 - \frac{BW}{2} \tag{5.8}$$

Substitution of Equation 5.8 into Equation 5.6 allows the calculation of cancellation bandwidth versus the cancellation level of the fundamentals. The cancellation bandwidth determines the feedback amplifier circuit useable bandwidth. The calculated bandwidths for n = 1, 3, 5, and 7 are shown below in Figure 5.3, where

$$\text{Attenuation} = 20\log\left(\left|2\cos\left(\left(n\frac{\pi}{2}\right)\left(1-\frac{BW}{2}\right)\right)\right|\right) \tag{5.9}$$

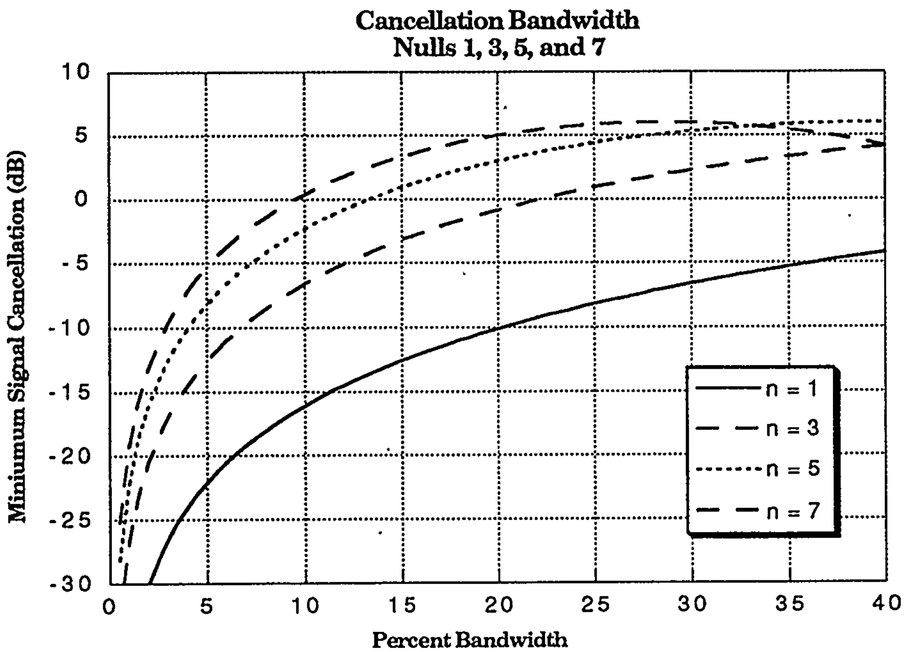

Figure 5.3 Cancellation Bandwidth for n = 1, 3, 5, and 7

Figure 5.3 illustrates the effect of the difference in delay between the two signals at the cancellation node on the cancellation bandwidth. For example, for a minimum 10 dB cancellation of the fundamental signal, a 20% bandwidth can be achieved at the first frequency null, but the bandwidth is reduced to 6.6%, 3.9%, and 2.9% for the nulls at n = 3, 5, and 7 respectively.

The effect of the loop delay may severely limit the bandwidth of the circuit in high frequency applications, where several cycles of energy may be stored in the feedback loop. This would result in the cancellation occurring at the higher order nulls as shown in Figure 5.3 resulting in a much narrower cancellation bandwidth.

5.1.2) Linear System Analysis

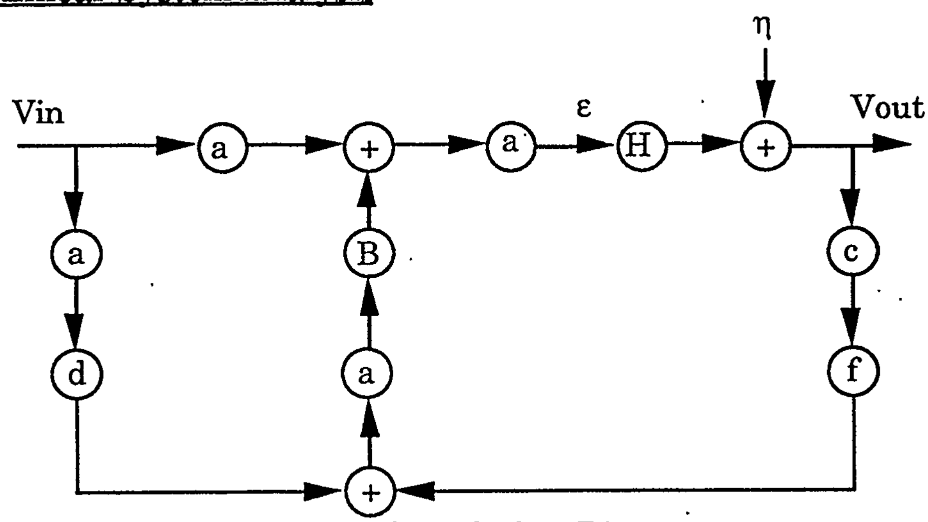

Figure 5.4 Signal Flow Diagram

Although the nonlinear nature of the amplifier does not allow traditional linear system analysis, the performance of the circuit can be approximated through the use of a linear amplifier stage with an additional noise term. This model is shown in the signal flow graph shown in Figure 5.4, where:

a = splitter/combiner loss,

H = Amplifier gain and delay characteristic, $H = he^{-j\omega\tau_h}$,

c = directional coupler attenuation,

d = lower path delay, $e^{-j\omega\tau_d}$,

f = variable attenuation,

B = loop amplifier and loop filter characteristic, $B(f)e^{-j\omega\tau_b}$,

η = intermodulation products.

The system equations for the signal flow diagram can be written as

$$V_{out} = \varepsilon H + \eta$$

$$\varepsilon = a^2 V_{in} + a^2 B(adV_{in} + cfV_{out})$$

$$V_{out} = a^2 HV_{in} + a^3 BdHV_{in} + a^2 BcfHV_{out} + \eta$$

$$V_{out} = \frac{a^2 H(1 + aBd)V_{in} + \eta}{\left(1 - a^2 BcfH\right)} \tag{5.10}$$

Note that the denominator of Equation 5.10 contains a difference term, rather than the sum which is the usual result given as the transfer function for a linear control system. This sign inversion is the result of using a combiner at the feedback circuit input node rather than the usual difference node. Equation 5.10 can be reduced if we consider the conditions necessary for the cancellation of the input signals at the lower summing node, which require

$$adV_{in} + a^2 cfHV_{in} = 0$$

or

$$acfh\left(e^{-j\omega\tau_h}\right) + e^{-j\omega\tau_d} = 0. \tag{5.11}$$

Equation 5.11 requires that

$$acf = \frac{1}{h} \qquad \text{and} \qquad \omega\tau_d = \omega\tau_h + n\pi \quad n=1,3,5,... \tag{5.12}$$

Substitution of Equation 5.12 into Equation 5.10 yields

$$V_{out} = a^2 H V_{in} + \frac{\eta}{\left(1 - aBe^{-j\omega\tau_h}\right)}. \tag{5.13}$$

Examination of Equation 5.13 shows that for perfect cancellation of the input signals, the overall circuit gain is unaffected by the feedback loop. This means that the reduction of circuit gain caused by the negative feedback has been eliminated. Although it was shown in section 5.2.1 that perfect cancellation of the input signal is not possible over a useable bandwidth, significant cancellation is possible which implies that the performance of the negative feedback amplifier can be improved.

Secondly, Equation 5.13 demonstrates that a reduction of the distortion products will still occur, and also that the amount of that reduction can be determined through the characteristic of the feedback filter and amplifier. This characteristic can be directly related to the Volterra kernels for the feedback amplifier derived earlier.

The amount of reduction in the distortion products is limited by the stability of the feedback loop, which is investigated in the next section.

5.1.3) Stability

In order to investigate the stability requirements, the circuit will be approximated by a linear system with delay. Since time domain techniques such as the Root Locus are not suitable for the analysis of a system with delay, the Nyquist plot was chosen to investigate the system stability.

The Nyquist plot is a frequency domain analysis which predicts the stability of the closed loop system through graphically examining the polar plot of the response of the open loop. For a system with delay such as the circuit examined here, the Nyquist criteria for a stability can be stated as follows: for the closed loop system to be stable, all intersections with the real axis of the Nyquist locus must occur to the right of the -1 + j0 point [22]. In this case, because of the sign inversion seen in Equation 5.10, the critical point becomes 1+j0, and the intersections of the locus with the real axis must appear to the left of the critical point.

As an example of the effects of delay on the system stability, consider the characteristic equation of Equation 5.13. The loop response is seen to be $aBe^{-j\omega\tau_h}$, which is a combination of the loop filter, feedback amplifier, and combiner responses. If the combiner loss is absorbed into the overall feedback amplifier characteristic, the loop response can be represented by a filter characteristic with gain and delay.

In order to determine the optimum filter response for the feedback loop, several different types and orders of filters were examined. Lowpass prototypes for Butterworth, Bessel, and Chebychev filters were transformed to bandpass prototypes using a lowpass to bandpass transformation, and the Nyquist plot of the responses examined for the maximum loop gain for different levels of loop delay. In this case, the maximum available loop gain is defined as the gain at which the Nyquist locus first intersects the critical 1 + j0 point on the real axis.

As an example of the procedure used, consider a second order Butterworth filter. In order to test the gain and delay effects, a second order Butterworth bandpass filter was derived by transforming the normalized lowpass, shown in Equation 5.14,

$$F(p) = \frac{1}{p^2 + \sqrt{2}p + 1} \tag{5.14}$$

to a bandpass characteristic using a standard lowpass to bandpass transformation [23],

$$p = \left(s + \frac{1}{s}\right)Q \tag{5.15}$$

where Q is defined as the inverse of the filter bandwidth. Equation 5.15 is substituted into Equation 5.14, and the result is scaled with gain and delay terms, resulting in Equation 5.16.

$$\beta(s) = \frac{1}{Q^2}\left(\frac{1}{s^4 + \frac{\sqrt{2}}{Q}s^3 + \frac{2Q^2+1}{Q^2}s^2 + \frac{\sqrt{2}}{Q}s + 1}\right) \bullet \mathrm{Gain} \bullet e^{-s\tau_{delay}} \tag{5.16}$$

The effect of the loop delay on the open loop feedback response can be illustrated by examining the Nyquist plot for Equation 5.16 for various gains and delays. First, with the gain set to unity, the loop response can be observed for different values of delay. The Nyquist plots for Equation 5.16 with delays of 0, π, 5π, and 9π radians are shown in Figure 5.5.

Examining Figure 5.5 shows that with the introduction of delay into the system, the locus of the Nyquist plot begins to spiral about the origin, with the number of intersections with the real axis increasing with increasing delay. In the limiting case, with enough delay the Nyquist locus will become essentially circular and the maximum loop gain will be limited to 1.

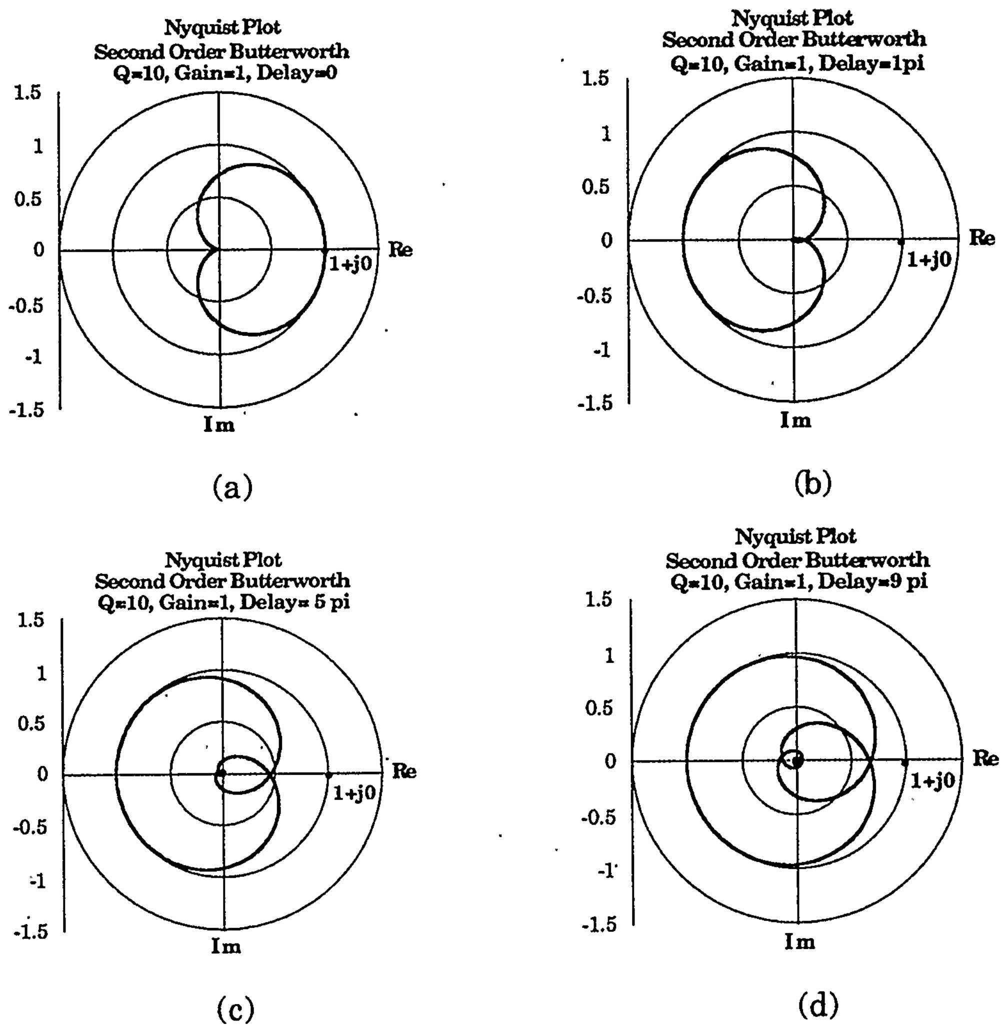

Figure 5.5 Nyquist Plots for Increasing Delay

Since the intent is to maximize the loop gain of the circuit, it is clear that the overall circuit delay must be minimized. Figure 5.6 shows the Nyquist plots for the maximum achievable gains for delays of 1π, 3π, 5π, and 9π radians, with gains of 18, 10, 6, and 3 dB respectively. The delays and gains result in a corresponding maximum reduction in distortion of 19, 12.4, 9.5, and 7.6 dB.

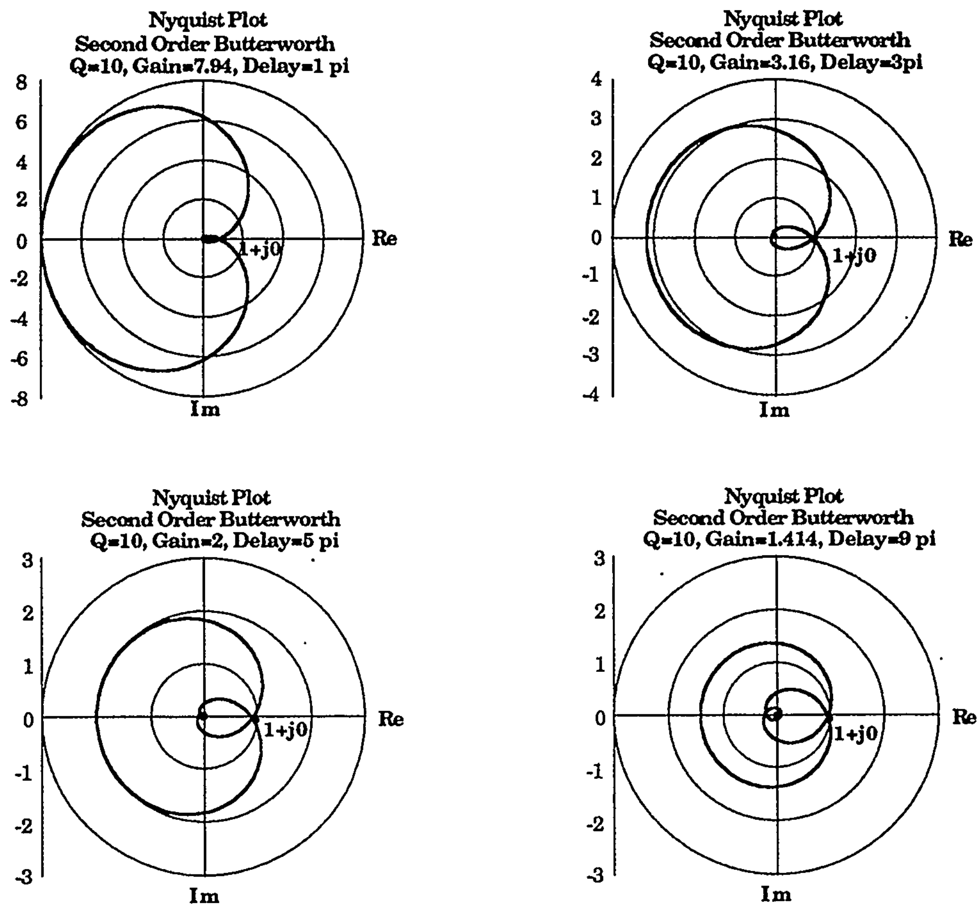

Figure 5.6 Nyquist Plots for Maximum Gain with Increasing Delay

This procedure was carried out for first, second, and third order Butterworth and Bessel lowpass prototype filters, as well as second and third order Chebychev filters with passband ripples of 0.1, 1.0, and 3 dB. The delays used were π, 3π, 5π, and 7π radians. The resulting maximum available loop gain in dB is given in Table 5.1.

Filter Q		3				5				10			
Loop Delay		π	3π	5π	7π	π	3π	5π	7π	π	3π	5π	7π
Butterworth	1	9.9	4.9	2.4	1.6	13.5	6.9	4.4	3.1	19.2	11.4	8.2	6.4
	2	8.9	2.7	1.1	.54	12.2	5.5	2.9	1.6	18.0	10.0	6.0	4.7
	3	4.0	1.0	0.3	0	5.7	2.4	1.1	0.4	7.3	3.6	3.0	1.9
Bessel	1	9.9	4.9	2.4	1.6	13.5	6.9	4.4	3.1	19.2	11.4	8.2	6.4
	2	6.9	2.2	1.1	0.6	10.5	4.2	2.3	1.5	15.9	8.2	5.4	3.7
	3	3.9	1.2	0.6	0.3	6.0	2.4	1.3	0.8	8.6	4.6	3.0	2.2
Chebychev													
ripple=0.1 dB	2	4.0	0.2	0	0	7.5	1.6	0	0	13.2	5.2	2.5	1.2
	3	1.5	0	0	0	2.9	0	0	0	4.4	1.9	0.9	0
ripple=1 dB	2	0	0	0	0	9.9	2.4	0	0	15.9	7.3	3.6	1.7
ripple=3dB	2	4.7	0	0	0	9.1	0.9	0	0	14.9	6.0	2.3	0

Table 5.1) Maximum Available Loop Gain (dB) For Butterworth, Bessel and Chebychev Filter Response

Examination of Table 5.1 shows that the maximum loop gain is obtained with the single pole Butterworth bandpass filter. It is also clear that the total amount of delay is a critical parameter for the circuit performance. In order to achieve useful reductions in the distortion level the total loop delay should be less than 5π radians, which may not be possible for high frequency amplifiers.

Another limitation is in the Q, or bandwidth, of the feedback loop, as the maximum loop gain is inversely proportional to the circuit bandwidth. Table 5.1 shows that levels of cancellation comparable to those achieved by the DSP techniques, such as 20 dB or greater reduction in IM_3, are only possible for circuits with a total delay of π radians and less than a 5% bandwidth. This limits the circuit applications to relatively narrow band systems such as cellular radio.

If we make some assumptions about the circuit operation, then we can make a prediction of the bandwidth / IM3 reduction trade off. The required assumptions are:

1) The cancellation node is operating at relative delay between the two signals of π radians, allowing the greatest cancellation bandwidth.

2) The minimum acceptable cancellation of the fundamentals in the feedback loop is 10 dB, giving a 20% maximum circuit bandwidth, as shown in Figure 5.3, and a maximum reduction in the amplifier gain of about 1 dB.

3) The feedback loop filter is a single pole Butterworth.

4) The cancellation of the fundamentals is large enough to neglect their effect, allowing us to consider the loop gain at the IM_3 frequency only.

5) The circuit bandwidth is the inverse of the Q of the Butterworth bandpass filter used in the feedback loop.

While assumption four makes the calculation much simpler, it is not entirely true and results in a slightly optimistic result. Now considering those frequencies that are at the -3dB points of the loop characteristic, a calculation of the minimum reduction in the IM_3 for a given bandwidth can be made using

$$\Delta IM_3 = 20\mathrm{Log}\left(\left|\frac{1}{1-\beta_1 h_1(f_{-3dB})}\right|\right)\ \mathrm{dB}. \tag{5.17}$$

Equation 5.17 has been plotted in Figure 5.7 for 3 dB bandwidths of 0 to 20 %, and for total circuits delays of π, 3π, 5π, and 7π radians.

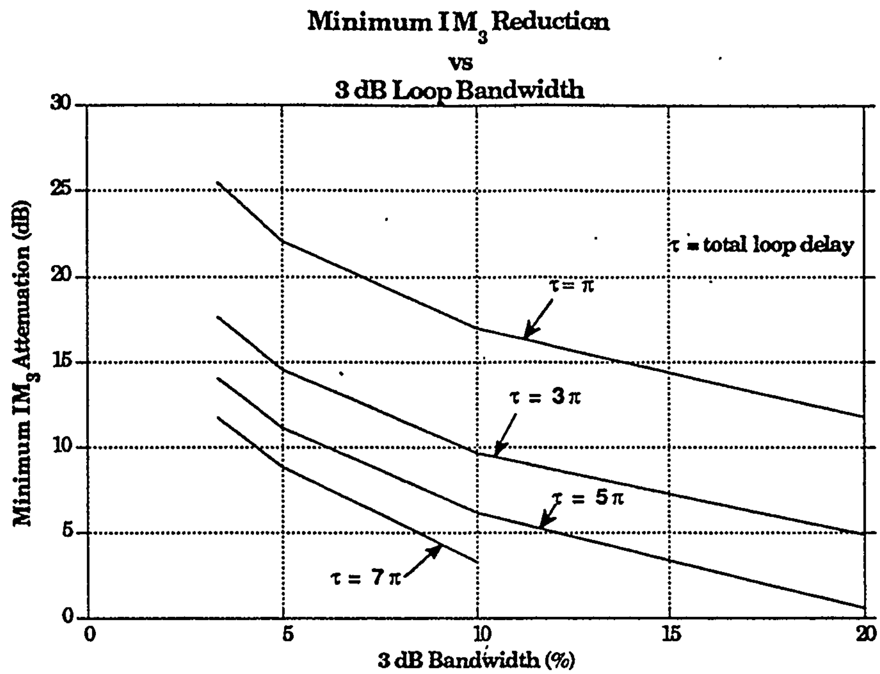

Figure 5.7 Minimum IM3 Reduction vs Circuit Bandwith

Chapter Six

Experimental Circuit, Measurements, and Results

This section deals with the construction of the test circuit, the experimental procedures used, and the test results obtained. The experiments address the cancellation bandwidth, reduction of the distortion products, and the circuit stability issues discussed in Chapters four and five. A comparison between the predicted and measured performance is also made.

6.1) Circuit Realization

In constructing the test circuit, it was decided to use available modules wherever possible. RF Minicircuits® was the primary choice due to the component availability and relatively low cost. It was necessary to build a custom variable attenuator and a bandpass filter in order to complete the circuit hardware requirements. Due to the type of circuit construction used, the delays inherent in the circuit became quite large, which resulted in relatively low test frequency of 305 MHz.

The final realization is given below in Figure 6.1, which shows the test circuit and corresponding test set up. The required delays for τ_1 and τ_3 were realized using lengths of coaxial cable.

6.1.2) Circuit Module Specifications

Σ1 RF Minicircuits ZA3PD-1.5 combiner

Frequency Range	500 - 1500 MHz
Isolation	20 dB
Insertion Loss	6.2 dB

Σ2,Σ3,Σ4	RF Minicircuits ZFSC -2-5 combiner		
		Frequency Range	10 - 1500 MHz
		Isolation	30 dB
		Insertion Loss	3.3 dB
Main Amp	RF Minicircuits ZHL-2-8 amplifier		
		Frequency Range	10 - 1000 MHz
		Gain	27 dB
		1 dB Compression Point	+29 dBm
		3rd Order IP	+38 dBm
FB Amp	RF Minicircuits ZFL 1000GH amplifier		
		Frequency Range	10 - 1000 MHz
		Gain (variable)	24 dB
		1 dB Compression Point	+13 dBm
		3rd Order IP	+25 dBm
Coupler	RF Minicircuits ZFDC-10-2 directional coupler		
		Frequency Range	10 - 1000 MHz
		Coupling	10.75 dB
		Insertion Loss	1.5 dB
		Directivity	30 dB

Note that although the frequencies used fell below the specified values for Σ1, the module performed satisfactorily with a slightly increased insertion loss over the specification given by RF Minicircuits. The values

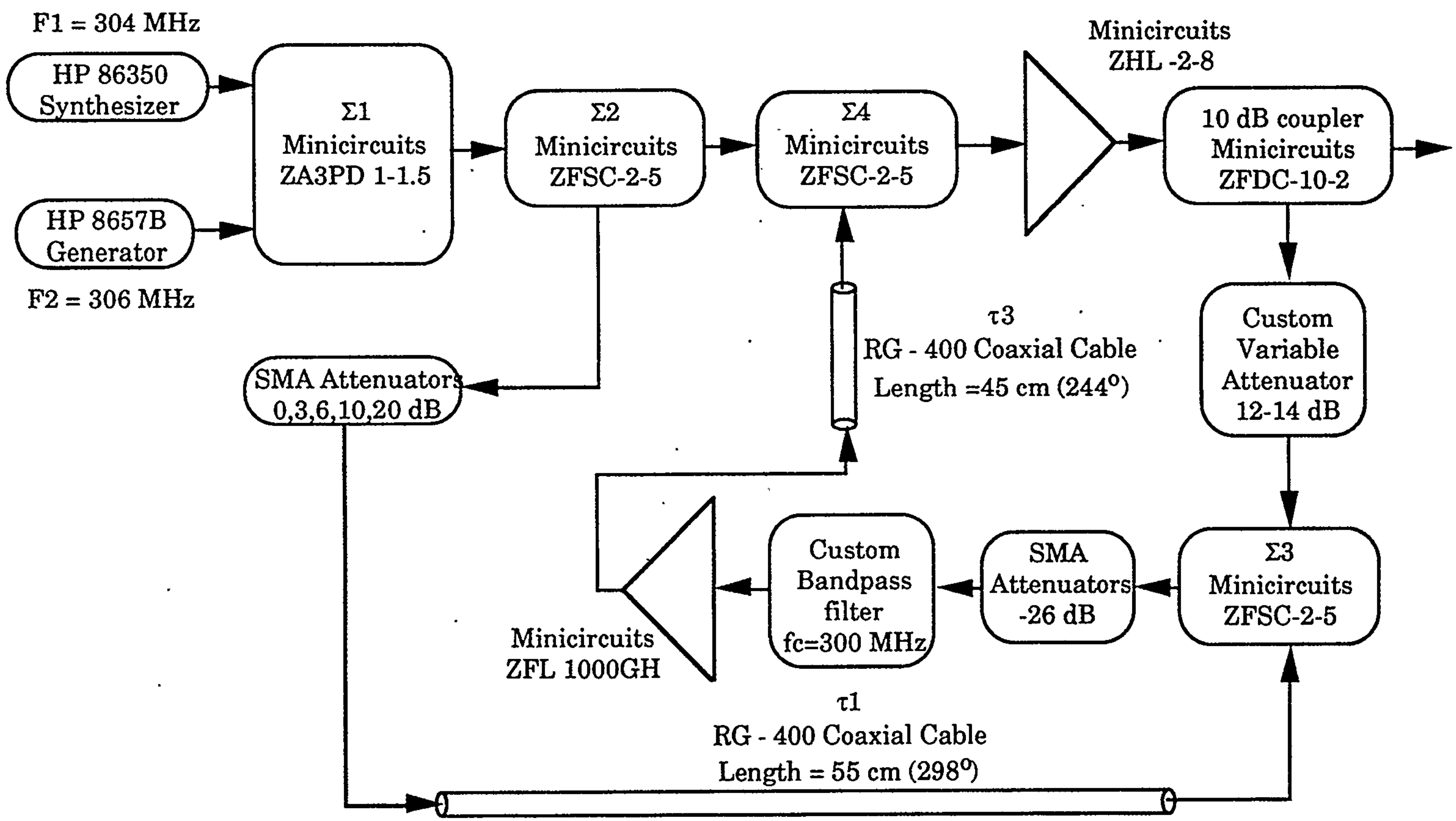

Figure 6.1) Experimental Circuit Realization

given for Σ1 in the specification above are measured results.

Although the commercial parts were satisfactory for most of the experimental circuit, it was necessary to develop a continuously adjustable attenuator and a bandpass filter centered on the cancellation circuit's passband.

6.1.3) Adjustable Attenuator

In order to achieve the required amplitude balance between the coupled output signal and the sampled input signal at Σ3, it was necessary to have a continuously adjustable attenuator with a fine resolution. Available commercial attenuators are indexed in 1 dB steps, which did not give the required level of cancellation at Σ3. To ensure good cancellation, a custom attenuator was constructed.

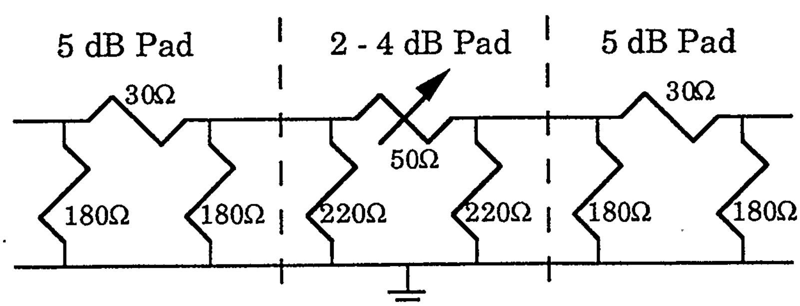

Figure 6.2 Adjustable Attenuator Circuit Diagram

The attenuator was built on FR4 fiberglass protoboard using surface mount resistors and a single 50 ohm potentiometer, with SMA connectors at the input and output ports. A 5 dB resistive pad is placed at each port of the attenuator in order to reduce the effects of the mismatch caused by the potentiometer. The result was a broad band attenuator with good return loss and a continuous adjustment range of 12 to 14 dB insertion loss. The circuit diagram is shown in Figure 6.2.

6.1.4) Bandpass Filter

In order to ensure circuit stability, and to isolate the effects of the fundamental and IM_3 feedback from the harmonics, it was necessary to place a bandpass filter in the feedback loop. In order to match the feedback loop's center frequency, which was determined by the delay inherent in the cancellation circuit, the filter's center frequency was set to 305 MHz. Again, because commercial alternatives were deemed to be either too expensive or have an excessively long delivery time, a custom filter was required. It was decided to construct a simple custom bandpass filter in order to demonstrate the principles of the circuit.

A single pole, quarter wave resonator filter was chosen due to its simplicity of construction. The equivalent circuit and its realization are shown below in Figure 6.3. The ceramic resonator is a quarter wave length of transmission line that has been shorted at one end. The transmission line is made up of a low loss, high dielectric constant material with an ε_r of 90, that has been coated with a conductive material. At the quarter wave frequency, the impedance appearing at the open circuit end of the resonator exhibits a high Q parallel resonance characteristic. In this case, the resonator used was a Murata Erie DRR060KER460T, with $f_c = 460$ MHz and a Q of 450.

The resonator was matched to 50 ohms through capacitive impedance transformers as shown in Figure 5.6. As the equivalent values of the resonator's C_0, L_0, and R are unknown, a circuit analysis and design was not performed.

The filter was built and tuned on the bench on FR4 board using surface mount capacitors and SMA connectors. Qualitatively, the filter's f_c is primarily determined by C_p, while the coupling, and hence the insertion loss and passband Q, are determined by C_s.

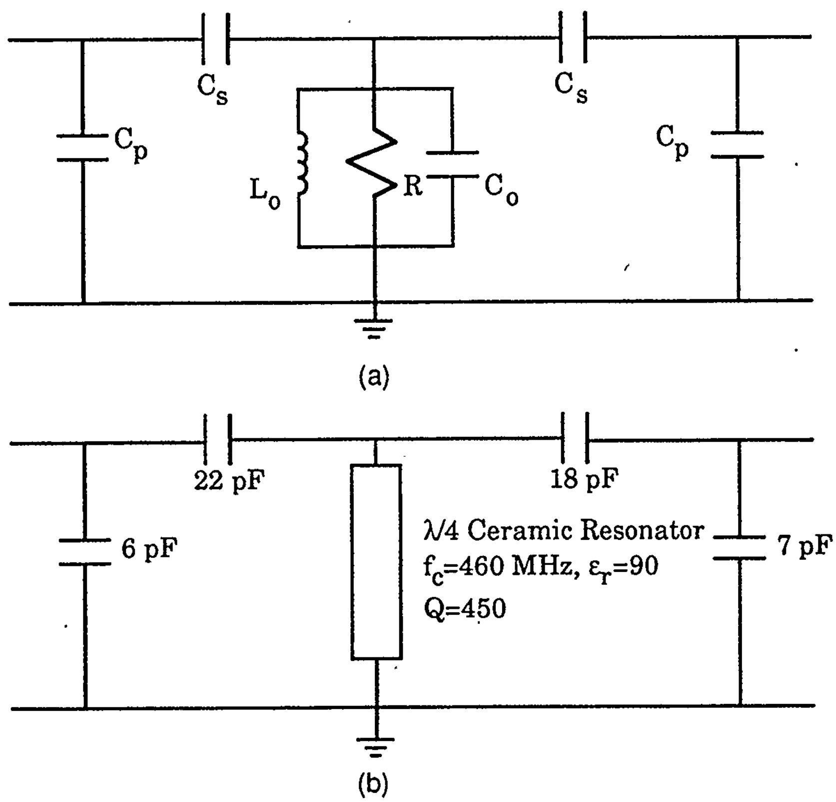

Figure 6.3 a) Filter Equivalent Circuit
b) Filter Circuit Diagram

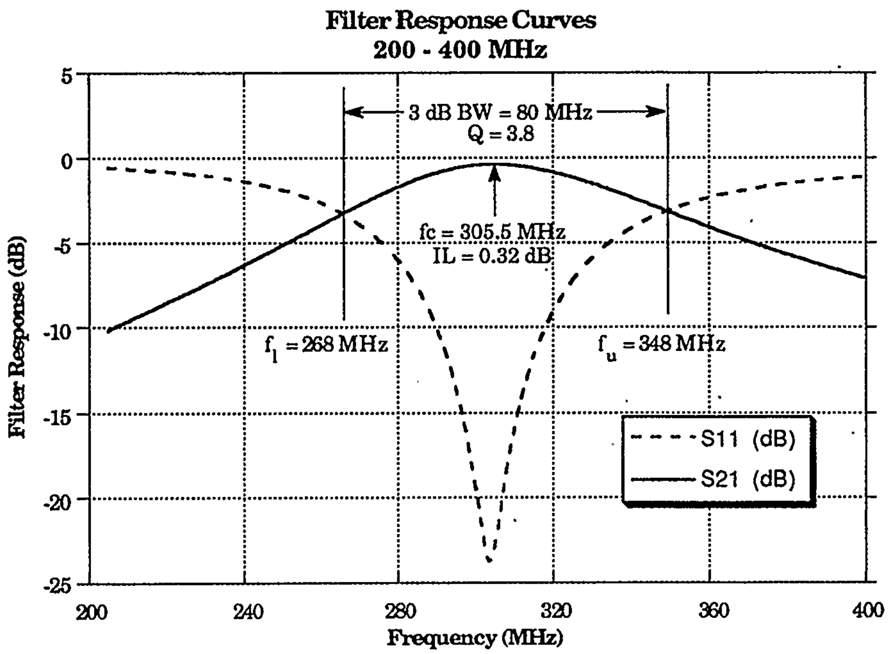

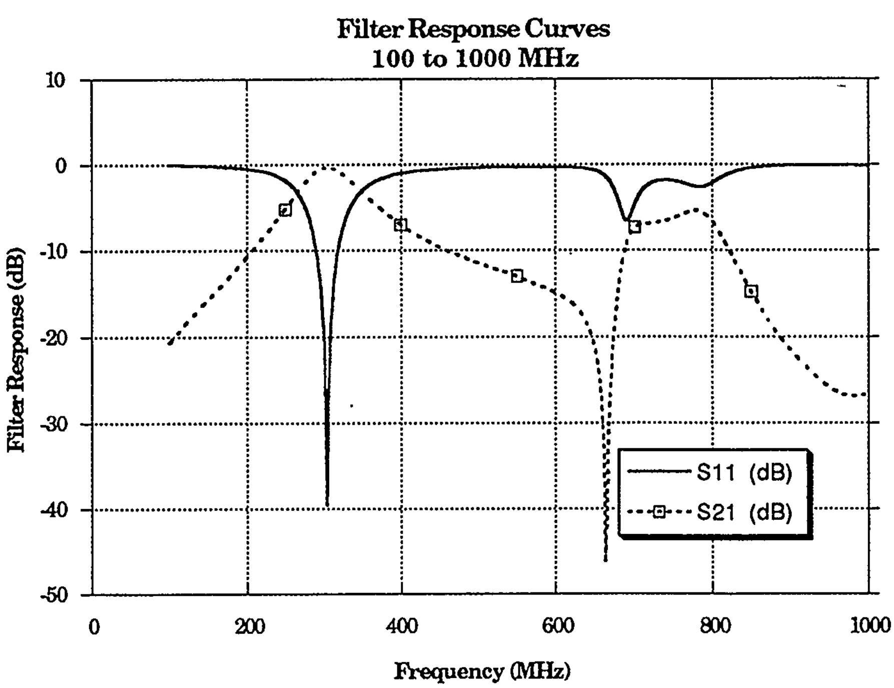

Figure 6.4 Bandpass Filter Response Curves

The filter passband and reflection loss were measured on a network analyzer, with the resulting plots shown in Figure 6.4. It is a characteristic of coupled quarter wave resonator filters to exhibit a spurious passband, which can be observed in Figure 6.4. In most systems the spurious passband falls outside the system passband but in this case, because of the high bandwidth of the Minicircuits components, the spurious response falls within the circuit's limits. This was initially a concern because it was felt that the spurious passband could have led to stability problems. This was disproved later in the experiment.

6.2) Experimental Procedure and Results

In order to prepare for the experiments, the circuit went through a two stage set up. In the initial stage, the feedback loop was tuned for stable operation, at a maximum loop gain, as a negative feedback amplifier centered at 305 MHz. The second stage was to tune the cancellation loop and attenuators such that optimum fundamental cancellation was achieved at a 305 MHz center frequency. This cancellation corresponds to a difference in delay of π radians between the two signals, as was discussed earlier.

During the construction of the cancellation loop, a single SMA adapter was inserted as a part of τ_1. This adapter was of the same phase length as the set of SMA attenuators which were to be used in the experiment to attenuate the feedforward of the input signal in order to vary the level of fundamental cancellation within the feedback loop.

6.2.1) Cancellation of Fundamentals

The initial set of measurements were intended to confirm the operation of the cancellation node Σ3, and to compare the results with those predicted in section 5.2.1.

A single constant amplitude low power tone, which was swept several times from 200 to 400 MHz, was input to the circuit and the resulting output captured on a spectrum analyzer that had been set for maximum hold on the trace. The relative delay was then increased from 1π radians to 3π and then to 5π radians and further measurements taken. The results were then normalized in amplitude to give a zero dB reference level, and plotted against Equation 5.6 with f_0=305 MHz. Both the measured and calculated results are plotted below in Figure 6.5, with good agreement being achieved in all cases.

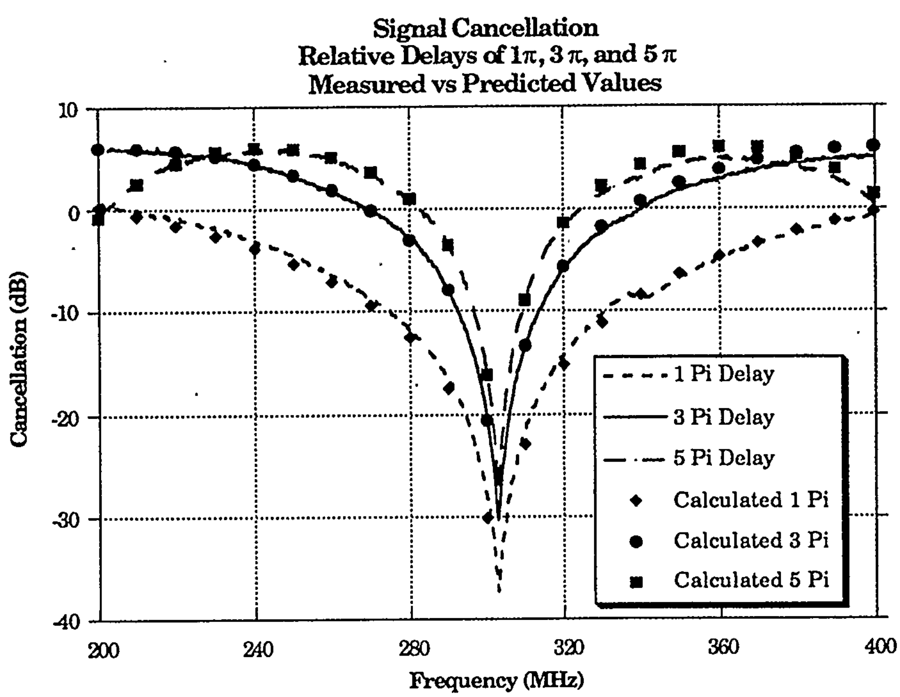

Figure 6.5 Measured vs. Predicted Signal Cancellation

The level of agreement between the measured data and predicted cancellation also supports the prediction of the cancellation bandwidth, which was given in Figure 5.3, as the same equation was used in both cases. The measurement also confirms that the circuit's cancellation node is operating at its optimum point, with only π radians difference in phase between the two input signals.

6.2.2) Circuit Performance Measurements

The second test was to measure the amplifier's output and IM_3 performance for open loop, closed loop, and closed loop with various levels of cancellation of the fundamentals at $\Sigma 4$. A two tone test was used with f_1=304 MHz and f_2 = 306 MHz, with the input signal power to the circuit ramped from -14 to + 6 dBm. The cancellation level was adjusted by inserting different values of SMA attenuators into the cancellation loop. Attenuator values of 0, 3, 6, 10, and 20 dB were used, resulting in cancellation levels of 30, 11.8, 7.5, 4.5, and 0.81 dB respectively for f_1 and f_2 at the output of $\Sigma 3$.

The amplitudes of the fundamentals and IM_3 frequencies, f_1, f_2, $2f_1$-f_2, and $2f_2$-f_1, were measured for the open loop, closed loop, and closed loop with cancellation. The resulting plots are shown below in Figures 6.6, 6.7, and 6.8. Figure 6.6 shows an example of a typical output spectrum measured for the two tone test for both the open and closed loop cases. Figures 6.7 and 6.8 give the measured results for the fundamental output power and the IM3 output power respectively. Only the information for f_1 (304 MHz) and $2f_1$-f_2 (302 MHz) have been plotted in figures 6.7 and 6.8 because of the symmetry of the results.

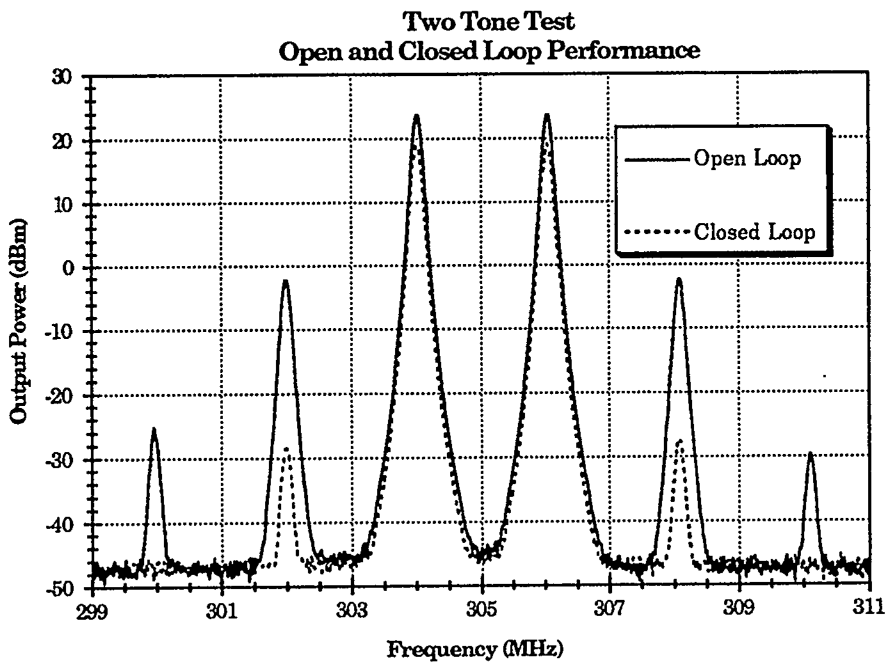

Figure 6.6 Two Tone Test Output Spectrum

Examination of Figures 6.7 and 6.8 yields three observations. The first is that the gain of the negative feedback amplifier can be modified through the cancellation of the input signal in the feedback loop.

The second observation is that there is a minimum level of distortion reduction even if the input signal is effectively completely canceled in the feedback loop. This is shown by the 30 dB cancellation case, where the output power is unaffected by the negative feedback, while there is still an 8 dB reduction in IM_3, which is equal to the loop gain. This supports the results of the Volterra series analysis of the feedback amplifier discussed in section 4.3.

Finally, it is clear that the effects of the feedback and cancellation are reduced as the amplifier begins to saturate, resulting in a convergence of the traces.

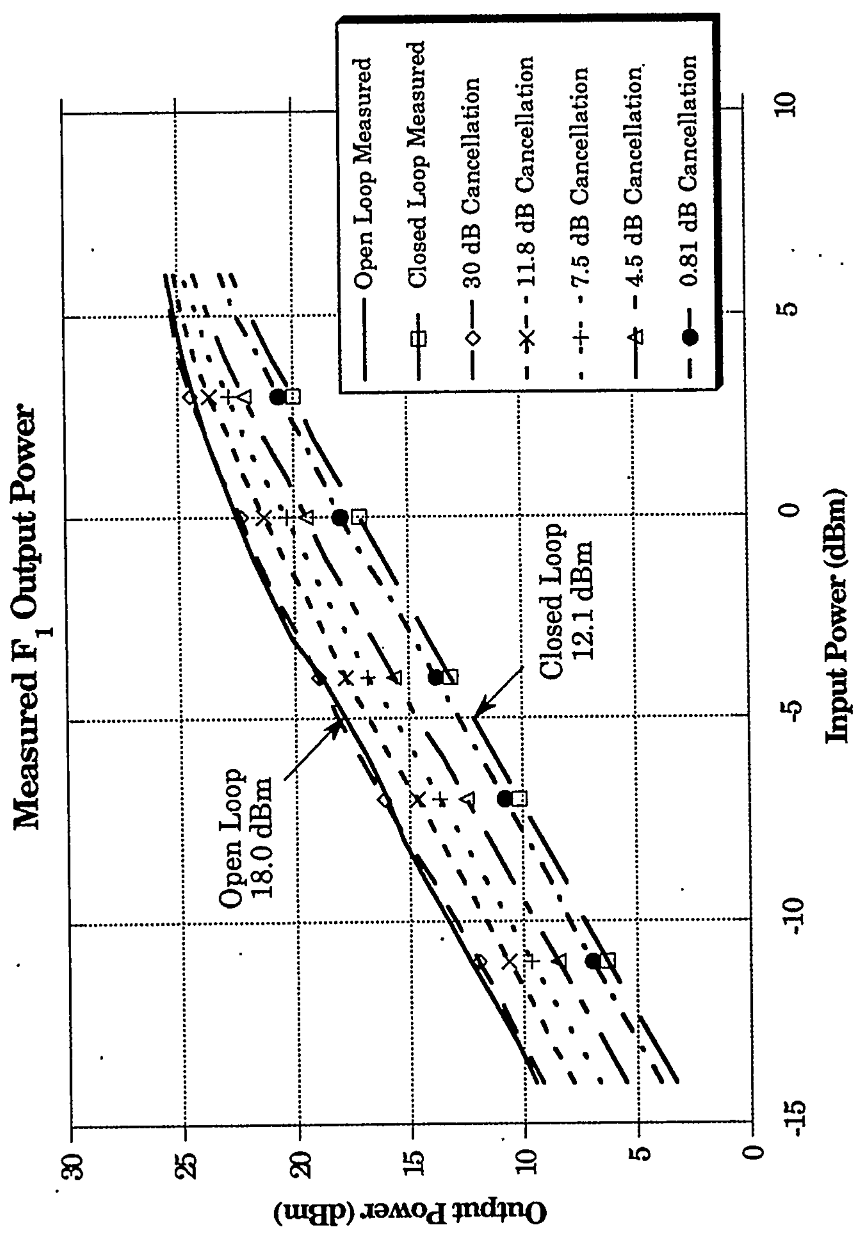

Figure 6.7 Measured Output Power at 304 MHz

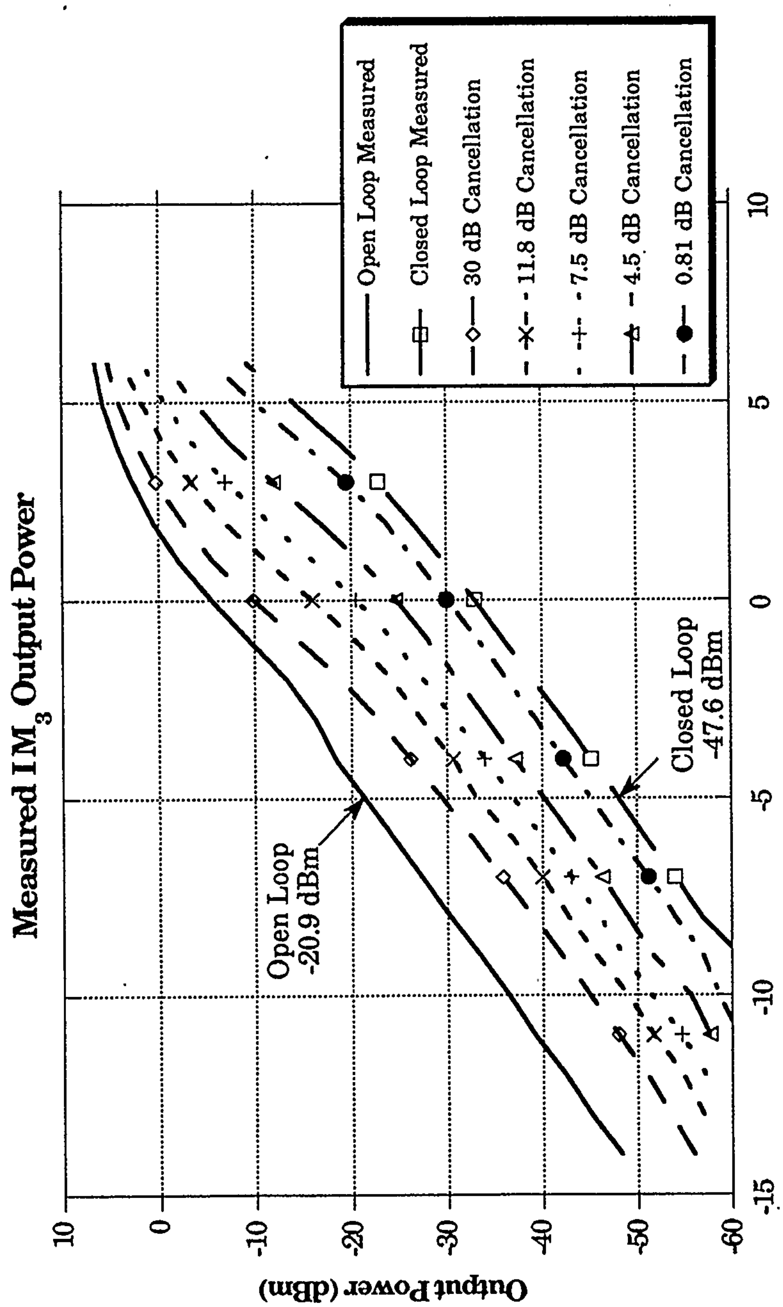

Figure 6.8 Measured Output Power at 302 MHz

Although Figures 6.7 and 6.8 give an an adequate representation of the circuit performance, a more accurate understanding can be obtained by plotting the circuit gain and distortion reduction normalized with respect to the F1 output power as in Figures 6.9 and 6.10.

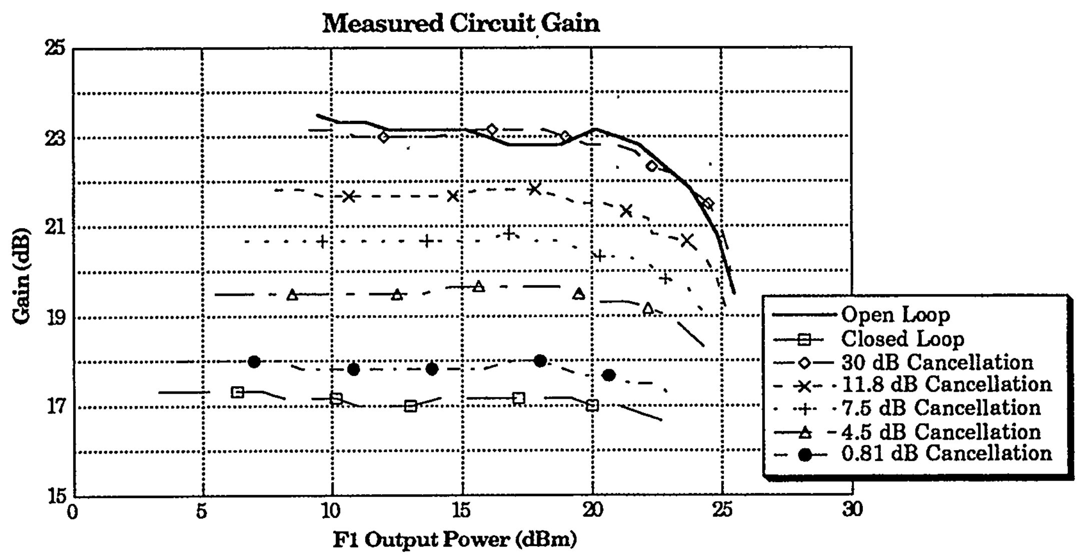

Figure 6.9 Measured Gain With Cancellation

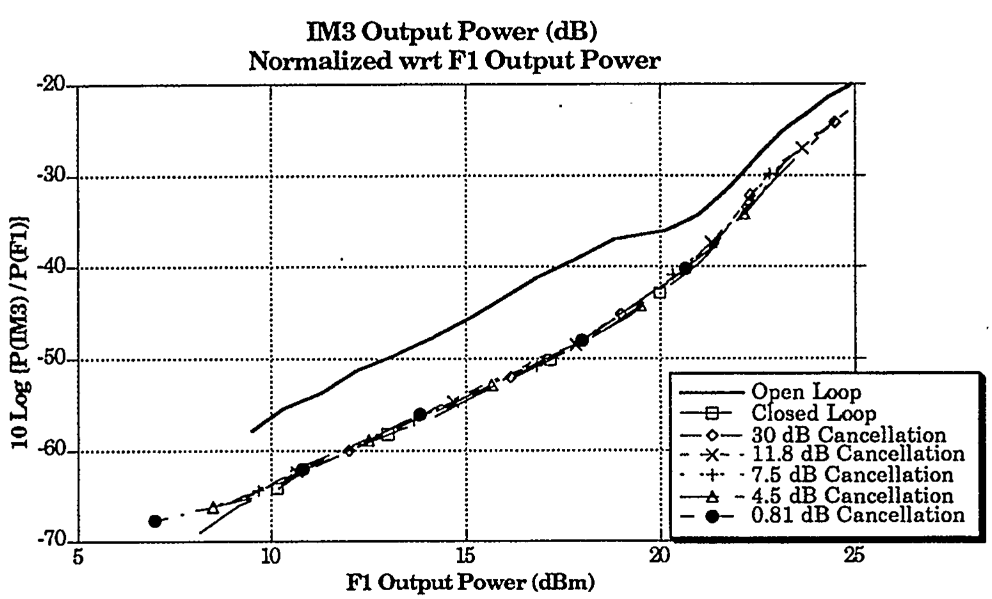

Figure 6.10 Normalized IM3 Output Power

Figure 6.9 clearly shows the effects of the cancellation of the fundamentals in the feedback loop and the resulting effect on the circuit gain. At the maximum cancellation point, the circuit gain is equal to the open loop case, while reducing the level of cancellation correspondingly reduces the circuit gain.

Figure 6.10 shows the IM_3 output power normalized with respect to the f_1 output power, and plotted against the f_1 output power. The normalization removes the reduction in the intermodulation products caused by the lower ouput power due to the the negative feedback. The remaining reduction, which is shown in Figure 6.10, is the effect of the loop gain of the circuit at the intermodulation frequency as shown in the Volterra series analysis.

When both figures are considered, it is clear that the circuit with cancellation can achieve a reduction in the distortion products equal to that of the closed loop amplifier without the subsequent reduction in circuit gain that is a result of the closed loop case.

It is clear then that the key parameter in the reduction of the intermodulation products is the loop gain of the circuit at the IM_3 frequency. The level of loop gain achievable is determined by the stability limits of the circuit.

6.2.3) Volterra Kernels

The next set of measurements were to determine the amplifier and feedback loop Volterra kernels. With reference to Figure 6.1, the input was taken to be at Σ4, while the open circuit output was taken to be at the output of the directional coupler, and the output of the feedback loop with various levels of cancellation was taken to be at the second input to combiner Σ4. All of the linear kernel measurements were taken on an HP 8510 network analyzer.

Cancellation	**H1(302 MHz) (dB)**	**H1(304 MHz) (dB)**	**H1(306 MHz) (dB)**	**H1(308 MHz) (dB)**
Open Loop		$23.5\angle -150.9^{\circ}$	$23.5\angle 144^{\circ}$	
Closed Loop	$0.094\angle 196^{\circ}$	$0.1155\angle 187^{\circ}$	$0.0998\angle 178^{\circ}$	$0.070\angle 168^{\circ}$
30 dB	$-30.0\angle 195^{\circ}$	$-30.1\angle 186^{\circ}$	$-30.5\angle 179^{\circ}$	$-30.1\angle 161^{\circ}$
11.8 dB	$-11.8\angle 196^{\circ}$	$-11.8\angle 185^{\circ}$	$-11.8\angle 178^{\circ}$	$-11.8\angle 164^{\circ}$
7.5 dB	$-7.4\angle 195^{\circ}$	$-7.4\angle 185^{\circ}$	$-7.5\angle 175^{\circ}$	$-7.5\angle 166^{\circ}$
4.5 dB	$-4.48\angle 195^{\circ}$	$-4.49\angle 185^{\circ}$	$-4.5\angle 176^{\circ}$	$-4.5\angle 167^{\circ}$
0.81 dB	$-0.81\angle 195^{\circ}$	$-0.81\angle 185^{\circ}$	$-0.81\angle 176^{\circ}$	$-0.82\angle 167^{\circ}$

Table 6.1 Linear Volterra Kernel Measurements

Although the linear Volterra kernels do not give enough information to model the amplifier's nonlinear response, they can be used to make an estimate of the relative performance between the open and closed loop cases. The reduction in the output of the fundamental tones can be written as

$$\Delta(f_1) = 20\log(|B_1|) \tag{6.1}$$

where

$$B_1 = \frac{1}{1-\beta_1 h_1(f_1)} \tag{6.2}$$

and the reduction in the output of the third order intermodulation tones can be written as

$$\Delta(2f_1 - f_2) = 20\log(B_3) \tag{6.3}$$

where

$$B_3(2f_1 - f_2) = \frac{1}{(1-\beta_1 h_1(f_1))^2} \bullet \frac{1}{1-\beta_1 h_1(f_2)} \bullet \frac{1}{1-\beta_1 h_1(2f_1 - f_2)}. \tag{6.4}$$

As an example, consider the performance for the amplifier as shown in Figures 6.7 and 6.8. At an input level of -5 dBm, the reduction in the output of the fundamental is shown in the figure to be 5.9 dB, while the reduction in the third order intermodulation product is shown to be 26.7 dB. In comparison, by converting the dB values to linear for the closed loop kernels given in Table 1, and then substituting them into Equations 6.2 and 6.4, B_1 and B_3 can be calculated as

$$B_1(304\text{MHz}) = \frac{1}{1-1.01339\angle 187^\circ} = 0.4976\angle -3.5^\circ$$

$$B_3(302\text{MHz}) = \frac{1}{\left(1-1.01339\angle 187^\circ\right)^2} \bullet \frac{1}{1-1.01156\angle 178^\circ} \bullet \frac{1}{1-1.01088\angle 196^\circ}$$

$$B_3(302\text{MHz}) = 0.06182\angle -10.5^\circ$$

which yields

$$\Delta(304) = 20\log(|B_1|) = -6.06\text{dB}$$

and

$$\Delta(302) = 20\log(|B_3|) = -24.2\text{dB}.$$

The result for f_1 is in good agreement with the measured results shown in Figure 6.7, while there is an error of 2.5 dB in the reduction of the $2f_1$ - f_2 intermodulation frequency as shown in Figure 6.8.

In order to fully predict the performance of the negative feedback amplifier using the Volterra series, it is also necessary to determine the third order kernels, as was shown in Equation 4.9. Although it is not possible to measure these kernels directly on the network analyzer, they can be extrapolated from the amplitude data gathered from the two tone test described in section 6.2.2. As the linear kernel $H_1(f_1)$ is known from the measurements, $H_3(f_1,f_1,-f_1)$ and $H_3(f_2,f_1,-f_2)$ can be determined through curve fitting equation 3.27 to the amplitude data gathered as discussed in section 6.2.2. As shown in equation 3.27, the outputs at f_1 and $2f_1$-f_2 can be written as

$$y_{(\omega_1)}(t) = |B_1|\cos(\omega_1 t + \angle B_1) \tag{6.5}$$

$$y_{(2\omega_1-\omega_2)}(t) = |B_2|\cos\left((2\omega_1 - \omega_2)t + \angle B_2\right)$$

(6.6)

where

(6.7)

$$B_1 = A_1H_1(j\omega_1) + \frac{3}{4}A_1^2A_1H_3(-j\omega_1, j\omega_1, j\omega_1) + \frac{3}{2}|A_2|^2A_1H_3(-j\omega_2, j\omega_1, j\omega_2)$$

and $$B_2 = \frac{3}{4}A_1^2A_2^*H_3(j\omega_1, j\omega_1, -j\omega_2) \tag{6.8}$$

If we assume a 50 ohm load, the power in dBm delivered to the load for either f_1 or $2f_1$-f_2 can be found as

$$P_{load} = \mathrm{Re}\left[10\log\left(10B^2\right)\right] \text{ dBm} \tag{6.9}$$

The values for $H3(f_1,f_1,-f_1)$ and $H3(f_2,f_1,-f_2)$ were found by using the measured value for H1(304 MHz) and curve fitting to the 304 MHz data using Equation 6.9. The constraints for the curve fit were that the resulting values must predict both the f_1 power output in dBm and the IM3 output power at 302 MHz in dBm. $H3(f_1,f_1,-f_1)$ and $H3(f_2,f_1,-f_2)$ were found to be

$$H3(f_1,f_1,-f_1) = 2 + j6 \quad \text{and} \quad H3(f_2,f_1,-f_2) = 5.5 + j8.$$

A comparison between the measured and calculated output powers for the open and closed loop cases have been plotted in Figures 6.9 and 6.10. The output powers for the closed loop calculations were found using the Volterra feedback amplifier Equations 4.3 and 4.9, shown again below as 6.10 and 6.11,

$$G_1(304\text{MHz}) = \frac{H_1(304\text{MHz})}{1+\beta_1 h_1(304\text{MHz})} \tag{6.10}$$

$$G_3(304\text{MHz}) = \frac{H_3(304\text{MHz})}{1+\beta_1 h_1(304\text{MHz})} \bullet \frac{1}{1+\beta_1 h_1(304\text{MHz})} \bullet \frac{1}{1+\beta_1 h_1(306\text{MHz})} \bullet \frac{1}{1+\beta_1 h_1(302\text{MHz})} \tag{6.11}$$

with the measured values of the feedback Volterra kernels shown in table 6.1 used for the loop gains in the equations. Examination of Figures 6.11 and 6.12 show good agreement between the calculated and measured values for the open loop and closed loop cases. A similar calculation was performed for the cancellation cases, also using Equations 6.10 and 6.11. Figures 6.13 and 6.14 also show good agreement between the measured and calculated cases for different levels of fundamental cancellation within the feedback loop.

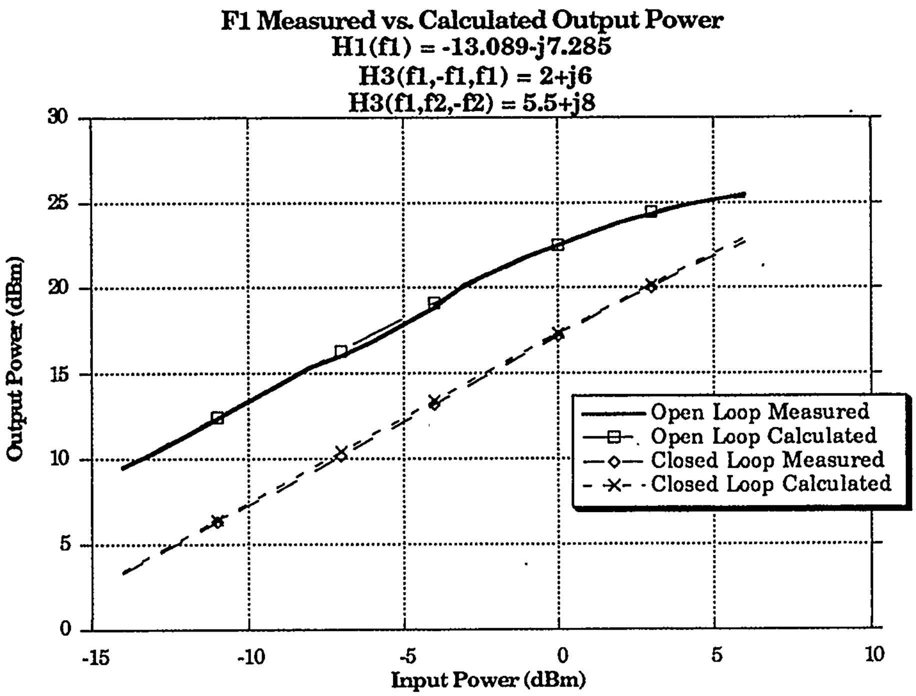

Figure 6.11 Measured vs Calculated F1 Output Power

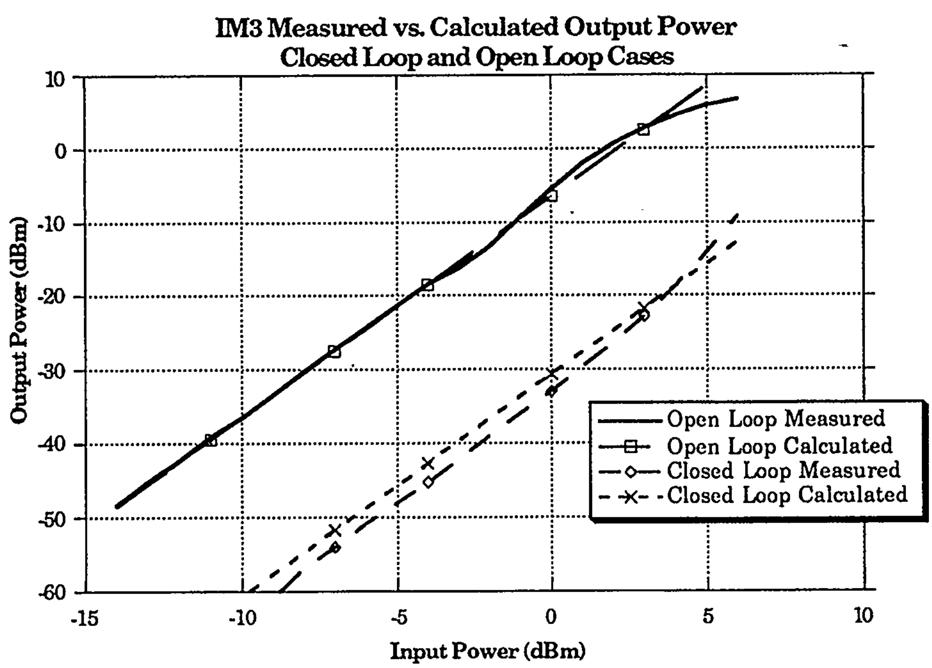

Figure 6.12 Measured vs Calculated IM3 Output Power

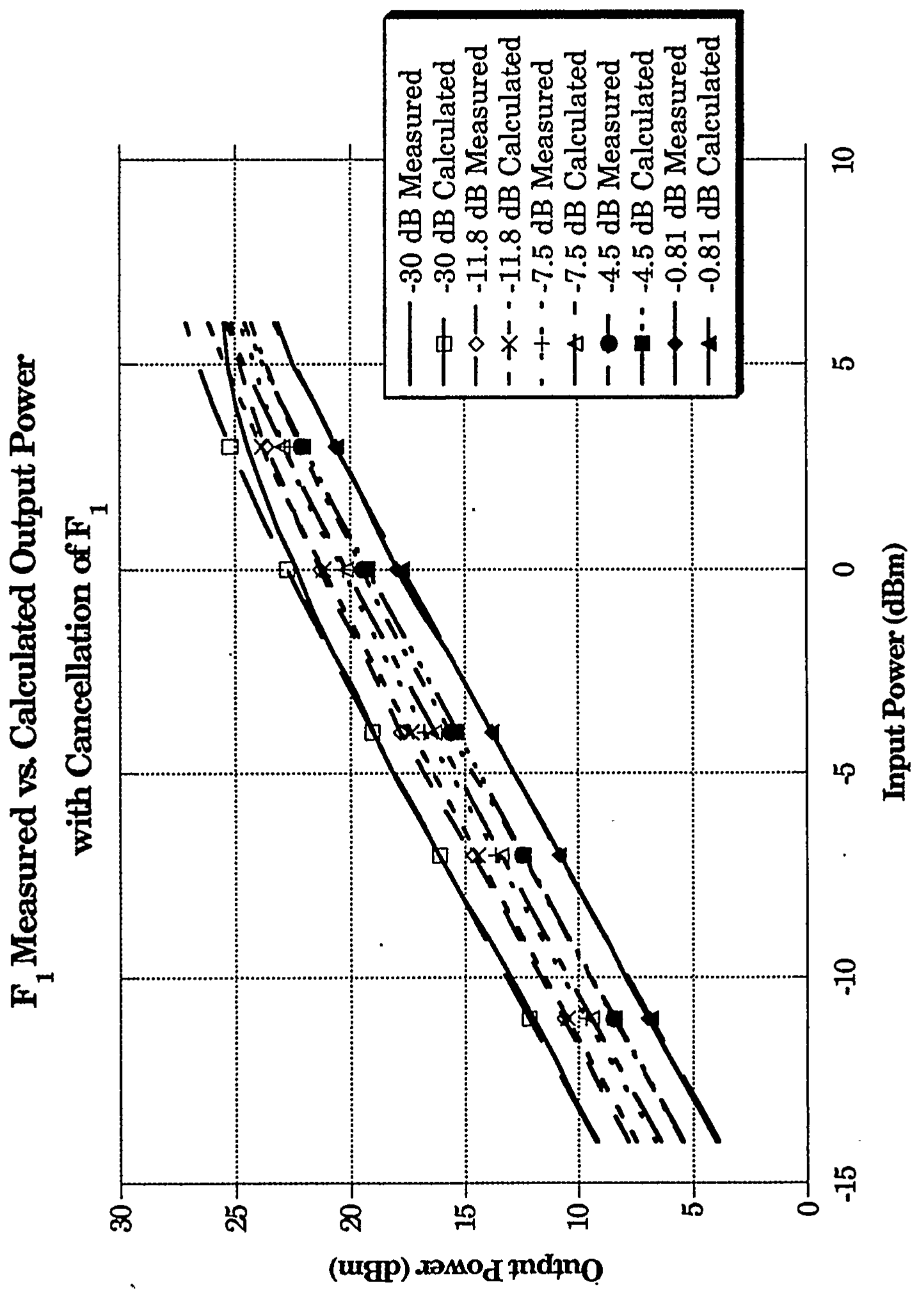

Figure 6.13 Measured vs Calculated F1 Output Power With Cancellation

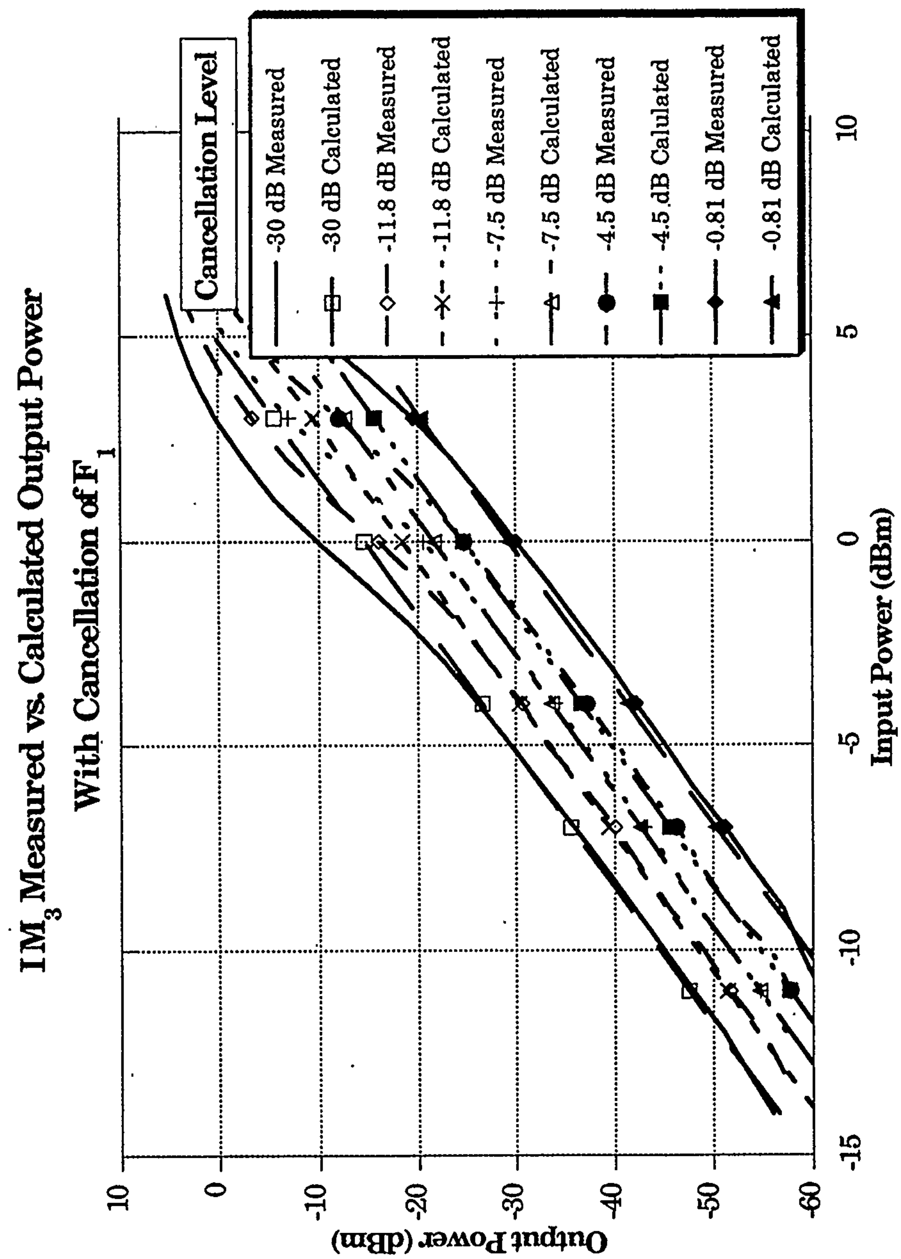

Figure 6.14 Measured vs Calculated IM3 Output Power With Cancellation

6.2.4) Loop Gain Measurements and Stability

In order to optimize the intermodulation product reduction, it was necessary to maximize the open loop gain. To investigate the stability and loop gain limits of the circuit, measurements were taken in both the stable and unstable circuit conditions.

The maximum loop gain condition was determined by increasing the gain of the feedback loop until a 260 MHz oscillation started, and then backing off the gain just enough to stop the oscillation. This condition was determined by observing the output of the circuit on a spectrum analyzer with the circuit input terminated in 50 ohms. The resulting noise spectra are shown below in Figures 6.15 and 6.16. Examination of these figures shows that the circuit has a tendency to oscillate at certain frequencies, which will be shown later to be related to the intersections of the Nyquist locus with the real axis as was discussed in Section 5.2.3.

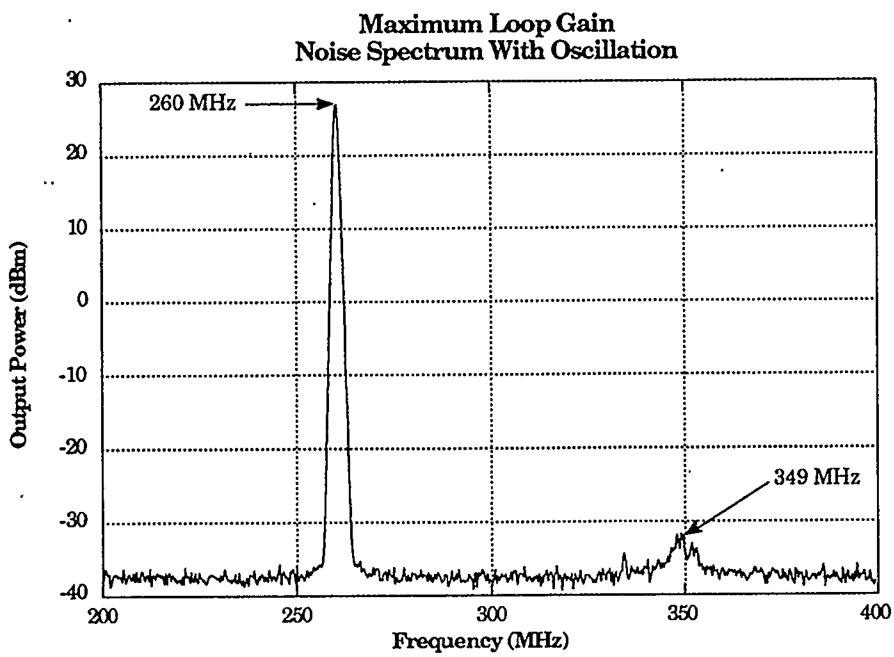

Figure 6.15 Noise Spectrum with Oscillation

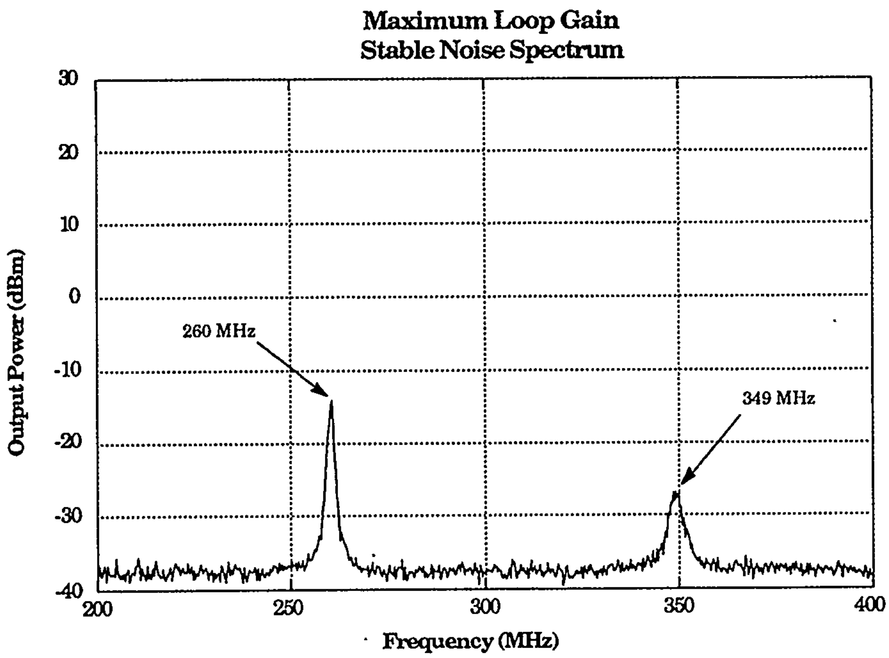

Figure 6.16 Noise Spectrum

Figures 6.16 and 6.17 show a 40 dB decrease in power at 260 MHz between the stable and oscillating conditions. The drop in power was very abrupt as the loop gain was decreased by about 0.5 dB, which indicated that, even though the noise floor indicates a tendency toward oscillation, the circuit was no longer oscillating. This was taken to be the maximum loop gain case.

With the maximum loop gain condition set, the next step was to observe the effects of the feedback loop characteristic and delays. An initial measurement was made of the bandpass filter without any delay, which is shown in Figure 6.17. The filter's spurious passband can be clearly observed in the Nyquist plot, but it will be shown in the next set of measurements that it does not play a role in determining the stability of the system.

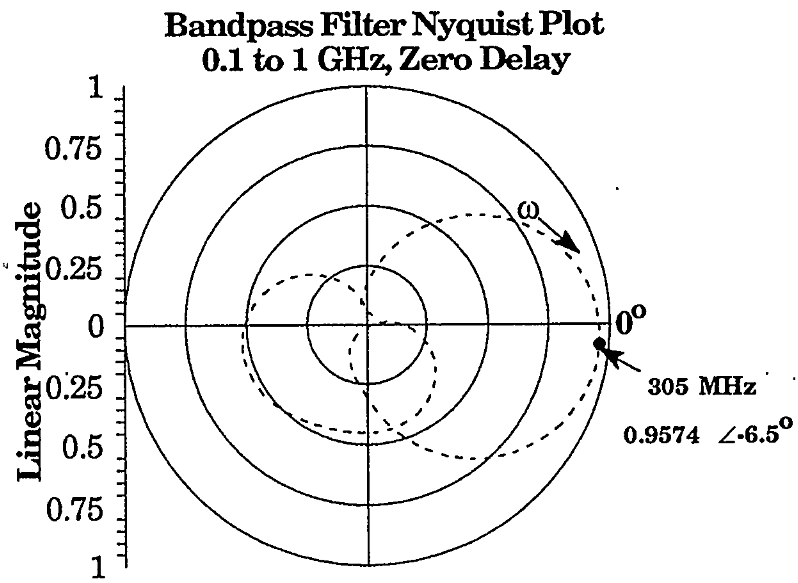

Figure 6.17 Bandpass Filter Nyquist Plot

The next measurements taken were of the open loop frequency response for both the no cancellation and maximum cancellation cases. The Nyquist plots of the resulting measurements are shown in Figures 6.18, 6.19, and 6.20.

Figure 6.18 shows the open loop response for the no cancellation case. When this figure is compared to the circuit noise plots shown in Figures 6.15 and 6.16, it can be seen that those frequencies which showed a tendency toward oscillation in the noise plots are the same as those frequencies at which the Nyquist locus intersects the real axis just to the left of the $1 + j0$ point. This result supports the shifting of the stability critical point from the standard value of $-1 + j0$ to $1 + j0$ as was discussed in the linear analysis given in Section 5.2.2. The figure also shows the values for the Volterra kernels for the negative feedback amplifier.

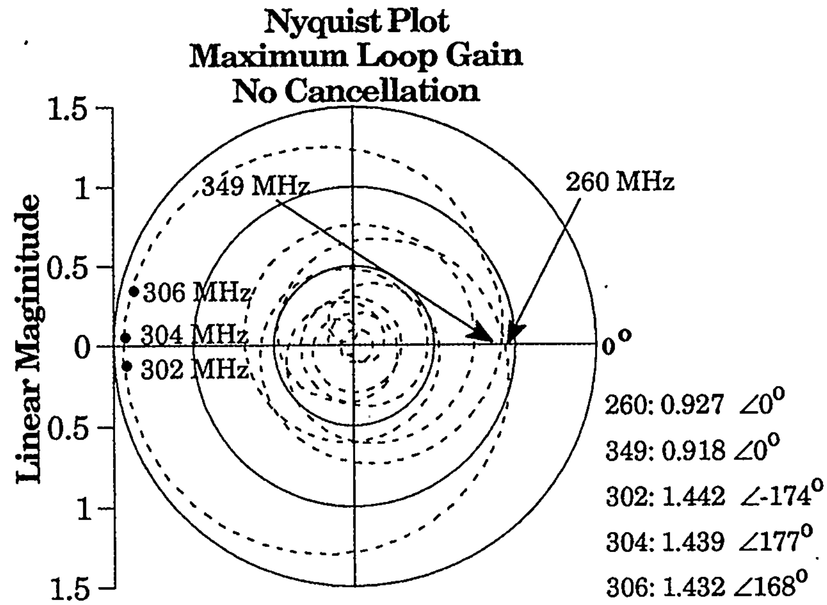

Figure 6.18 Open Loop Nyquist Plot, No Cancellation

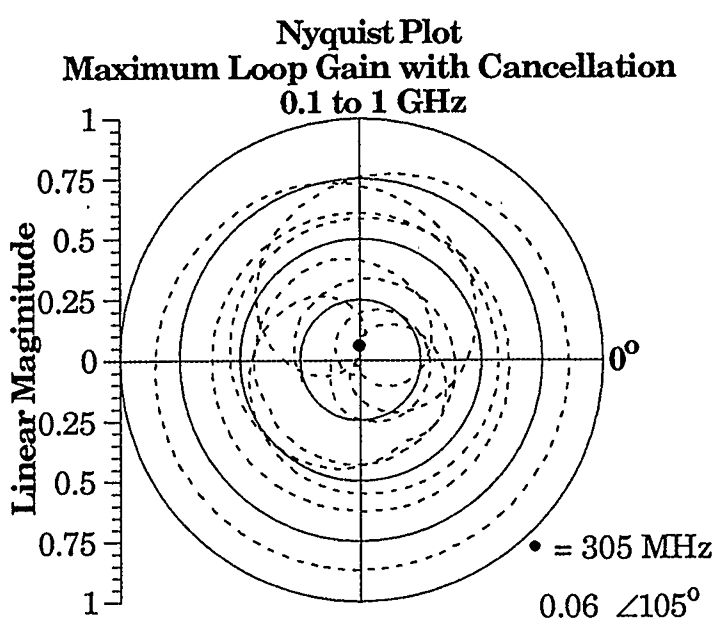

Figure 6.19 Open Loop Nyquist, Maximum Cancellation

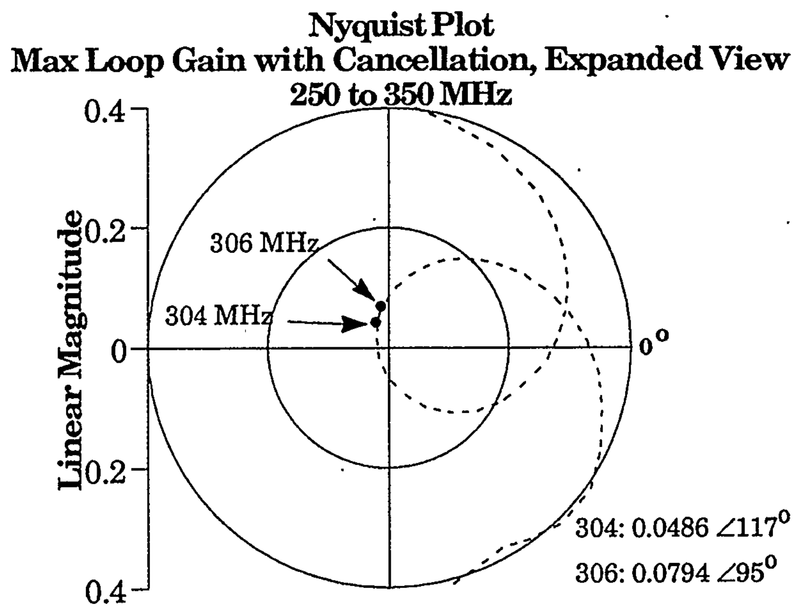

Figure 6.20 Expanded Open Loop Nyquist Plot, Maximum Cancellation

Figure 6.19 shows the effect of the addition of the cancellation of the fundamentals to the feedback loop. In order to see these effects, the information was replotted in Figure 6.20 in an expanded scale with the frequency range limited to 250 MHz to 350 MHz. It can be seen in Figure 6.20 that the loop gain for the fundamentals has been reduced by more than 20 dB.

Examination of the Nyquist plots confirms that the key parameter in determining the loop gain, and hence the reduction in the IM products, is the characteristic of the loop filter. In order to improve the response of the circuit, it would be necessary to either reduce the level of circuit delay or to modify the amplitude/phase characteristic of the filter in order to reduce the magnitude of the loop gain at the intersections with the real axis.

Chapter Seven

Conclusions and Future Work

The analysis and experimentation have clearly demonstrated that the intermodulation products of a mildly nonlinear amplifier can be reduced through the use of negative feedback without the loss of gain that is characteristic of the standard negative feedback amplifier. Alternatively, the proposed circuit would allow an increase in output power from the amplifier for a given level of intermodulation output power.

It was also demonstrated that the Volterra series and the resulting nonlinear transfer functions can be used in the analysis and prediction of the amplifier's performance, by using only the system level parameters. Of particular interest is the use of the linear Volterra kernels to predict the effect of feedback on the fundamental and third order intermodulation products. The linear kernels can be easily measured on a network analyzer and the amplifier's relative performance predicted using two equations.

The circuit proposed has limitations and tradeoffs in useable bandwidth and degradation of the amplifier gain, which are dependent on the total delay within the feedback loop, the operational class of the amplifier, and the reduction of the fundamentals in the feedback loop achieved at the cancellation node. The relatively narrow bandwidth of the circuit would make it unsuitable for broadband applications, but could be used in a narrow band application such as digital cellular.

Although the prototype circuit successfully demonstrated the principle of the circuit, the 8 dB reduction in the intermodulation products cannot be considered adequate considering the levels of reduction achieved by the Cartesian Feedback or the Adaptive Linearization techniques discussed in Chapter 2. The prototype circuit does compare favorably though in its simplicity and ease of implementation.

Future work would focus on both the reduction of the total circuit delay, and the improvement of the response characteristic of the feedback loop. The reduction of the circuit delay would be accomplished through the design of circuit using discrete components, which would minimize the delays seen in the experiment. If reduction in delay was great enough, the phase shift in the feedback network would be reduced enough to allow for a greater loop gain and hence an improved level of linearization.

The improvement of the response characteristic of the feedback loop would require either the development of bandpass filter that was optimized for this application, such that its magnitude/phase response would allow for a greater loop gain, or the use of a nonlinear element in the feedback loop to tailor the magnitude/phase response. In either case the focus would be to increase the stability of the circuit such that a greater loop gain could be used resulting in a greater level of distortion reduction.

References;

1. C.C. Hsieh, "Linear Amplification Techniques in 2 GHz Microwave Radios," NTC '77, pp. 16:3-1 to 16:3-3.

2. R.D. Stewart, F.F. Tusubira, "Feedforward Linearization of 950 MHz Amplifiers," IEE Proceedings, Vol. 135, No. 5, pp. 347-350, October 1988.

3. P.D. Lubell, W.B. Denniston, R.F. Herz, "Linearizing Amplifiers for Multi-Signal Use," Microwaves, April, 1974.

4. F.H. Raab, "Efficiency of Outphasing RF Power Amplifier Systems," *IEEE Trans. on Communications*, Com-33, No. 10, pp. 1094 - 1099 October 1985.

5. D.C. Cox, "Linear Amplification with Nonlinear Components," *IEEE Trans on Communications*, Vol. Com-22, pp 1942-1945, December, 1974.

6. A.Bateman, D.M. Haines, and R.J. Wilkinson, "Linear Transceiver Architectures," IEEE Vehicle Technology Conference, pp. 478-484, June 1988.

7. E.Ballesteros, F.Perez, and J. Perez, "Analysis and Design of Microwave Linearized Amplifiers Using Active Feedback," *IEEE Trans. on Microwave Theory and Techniques*, Vol-36, No. 3, pp. 499 - 504, March, 1988.

8. T. Arthanayake, and H.B. Wood, "Linear Amplification Using Envelope Feedback," *Electronics Letters*, Vol.7, No. 7, April, 1971.

9. V.G. Lavrushenkov, G.V. Novikov, and I.V. Chgunov, "The Features of Using Balanced Envelope Feedback in Power Amplifiers," *Radiotekhnika*, No. 3, pp. 89-90, 1989.

10. T. Nojima, T. Konno, "Cuber Predistortion Linearizer for Relay Equiment in 800 MHz Band Land Mobile Telephone System," *IEEE Trans. on Vehicular Technology*, Vol VT-34, No. 4, pp. 169 - 177, November, 1985.

11. N. Imai, T. Nojima, and T. Murase, "Novel Linearizer Using Balanced Circulators and Its Application to Multilevel Digital Radio Systems," *IEEE Trans. on Microwave Theory and Techniques*, Vol. 37, No. 8, pp. 1237 - 1243, August, 1989.

12. M. Nannicini, P. Magni, and F. Oggionni, "Temperature Controlled Predistortion Circuits for 64 QAM Microwave Power Amplifiers," *IEEE Microwave Theory and Techniques Conference Digest,* pp. 99-102, 1985.

13. A.A. Saleh, and J. Salz, "Adaptive Linearization of Power Amplifiers in Digital Radio Systems," *The Bell System Technical Journal*, Vol. 62, No.4, April 1983

14. Y. Nagata, "Linear Amplification Technique for Digital Mobile Communications," Proceedings of the IEEE Vehicular Technology Conference, pp. 159-164, 1989.

15. J. Cavers, "Amplifier Linearization Using a Digital Predistorter with Fast Adaptation and Low Memory Requirements," *IEEE Trans. on Vehicular Technology,* Vol. 39, No.4, November 1990.

16. A.S. Wright, and B. Durtler, "Experimental Performance of an Adaptive Digital Linearized Power Amplifier," *IEEE Trans. on Vehicular Technology*, Vol. 40, No. 4, November 1992.

17. Y.J. den Otter, *Adaptive Linearization of Power Amplifiers for Digital Cellular Radio*, Masters Thesis, Department of Electrical Engineering, University of Alberta and TR Labs, Edmonton, Alberta, 1992.

18. T.T. Ha, *Solid-State Microwave Amplifier Design*, New York: Johns Wiley & Sons, Inc.,1981.

19. R.B. Parente, "Nonlinear Differential Equations and Analytic System Theory," *SIAM Journal of Applied Mathematics*, Vol 18, No. 1, pp. 41 - 65, January, 1970.

20. S.Narayanan, "Application of Volterra Series to Intermodulation Distortion Analysis of Transistor Feedback Amplifiers," *IEEE Trans. on Circuit Theory*, Vol. CT-17, No.4, pp. 518 - 527, November 1970.

21. A.M. Khadr, *Distortion in High Frequency Transistor Amplifiers*, Masters Thesis, Department of Electrical Engineering, University of Calgary, Calgary, Alberta, February, 1973.

22. B.C. Kuo, Automatic Control Systems, 4 ed., pp. 558-593, Prentice Hall, 1982.

23. F.F. Kuo, Network Analysis and Synthesis, 2 ed., pp. 365-411, John Wiley and Sons, 1962.

24. D.D. Weiner, and J.F.Spina, Sinusoidal Analysis and Modelling of Weakly Nonlinear Circuits, Van Nostrand Reinhold Company, 1980.